The Dissertation Committee for Abraham Arceo Certifies that this is the approved version of the following dissertation:

Thermally Induced Transitions in Polymer Thin Films

Committee:

Arumugam Manthiram, Supervisor

Peter F. Green, Co-Supervisor

Isaac C. Sanchez

Harovel G. Wheat

Venkat Ganesan

Thermally Induced Transitions in Polymer Thin Films

by

Abraham Arceo, B.S.; M.S.

Dissertation

Presented to the Faculty of the Graduate School of

The University of Texas at Austin

in Partial Fulfillment

of the Requirements

for the Degree of

Doctor of Philosophy

The University of Texas at Austin

August 2007

Dedication

To my parents, Enrique and Silvia.

Acknowledgements

I would like to express my gratitude to all the people who have, one way or another, been present throughout this important stage of my life. I start by thanking Dr. Peter F. Green for giving me the chance to collaborate with him. It has been a valuable experience to work with a person who not only is committed to academic excellence, but also takes a personal interest in the development of each of his students. At the same time, I want to thank my fellow group members, for making of this experience such a memorable one. Having been surrounded by such a diverse, talented group has been enriching both academically and personally. I also want to thank my co-advisor Dr. Arumugam Manthiram and professors Dr. Harovel Wheat, Dr. Venkat Ganesan, and Dr. Isaac Sanchez for their guidance in the preparation of this manuscript while serving as members of my dissertation committee.

An important part of my life while on graduate school has been the continuous support and help from my friends in Austin, Ann Arbor and Mexico. I always felt encouraged, and sometimes even pampered by them, and for that I am profoundly grateful.

I want to thank my family, for their love and continued support. They have given me the strength to pursue my goals, and have always been enthusiastic about my endeavors. This achievement is as much theirs as it is mine.

I also want to thank the Meli Thompson family, who has taken me in as one of their own from the start. Throughout the years they have been a source of guidance and support for me. I feel really fortunate to have them in my life.

Finally, I want to thank my wife Luciana who has been with me every step of the way during this PhD. Having studied with her has been a wonderful, exciting experience. Her love, support and insightful approach to research have been essential to me all these years.

Thermally Induced Transitions in Polymer Thin Films

Publication No._____

Abraham Arceo, PhD

The University of Texas at Austin, 2007

Supervisors: Arumugam Manthiram and Peter F. Green

Polymers, by virtue of their chemical composition and molecular architecture, exhibit a diverse range of microstructural features and properties. As thin films, due primarily to effects associated with confinement and interfacial interactions, their properties may be film-thickness dependent. The significance of their thickness-dependent behavior is underscored by the fact that polymer films are of technological interest in areas that include, sensors, catalysts and organic electronics. One challenge associated with the use of thin film polymers is to understand the role of confinement and interfacial interactions on thermally induced transitions, such as vitrification and various morphological transitions. To this end, the work presented in this dissertation focuses on the behavior of thermally induced transitions in two thin film polymer-based systems: (1) an A-b-B diblock copolymer which can undergo a disorder-to-order transitions (ODT), wherein the ordered state exhibits varying geometrical symmetries, depending on the relative volume fractions of the A and B components; (2) an amorphous polymer filled with particles of nanoscale dimensions.

The first of three problems examined is the influence of supercritical carbon dioxide ($scCO_2$) on the order-disorder transition of thin film symmetric A-b-B diblock copolymer systems. We show that the transition $(\chi N)_{ODT}$, where χ is the energetic A-B Flory-Huggins interaction parameter and N is the total degree of polymerization of the

copolymer, of the thin film decreased ~ 20% compared to the bulk; the decrease was more significant in $scCO_2$ environments. The decrease of $(\chi N)_{ODT}$ in $scCO_2$ is contrary to observations in bulk copolymer-$scCO_2$ systems where the effective A-B interactions are weaker, hence the condition for the transition increases to higher $(\chi N)_{ODT}$ values. With regard to the second problem, we show for the first time experimentally that nanoparticles induced order into thin films of a symmetric A-b-B diblock copolymer at temperatures below the bulk ODT. Finally, we examine the influence of polystyrene (PS) grafted nanoparticles on the glass transition of PS films of varying molecular weight and thickness. We demonstrate that by controlling spatial distribution of nanoparticles, through driving forces of entropic origin, the glass transition temperature of the film can be changed drastically, as much as tens of degrees.

Table of Contents

List of Tables

List of Figures

Chapter 1: Introduction

1.1 Motivation and Research Objectives

Since they were first controllably synthesized, the use of polymers has pervaded nearly every aspect of human activity. The first synthetic polymer, the bakelite, was used in applications where its insulating properties were needed. As the synthetic procedures were refined and the physics of polymers were better understood, it became possible to generate entire families of materials whose properties could be tailored for specific applications. These long-chain molecules are synthesized in a range of architectures: linear chains, multi arm star chains, cyclic molecules, dendrimers, branched and cross-linked macromolecules. Polymers exhibit a rich diversity of morphologies/microstructures determined largely by molecular architecture, chemical constituents and various processing conditions. In many cases fillers are added to the polymer during processing in order to achieve certain properties not achievable by the pure polymer. The applications are diverse, from structural applications such as automobile bumpers to active components in microelectronic devices and sensors. More recently, many cutting-edge applications, such as sensors, lithography, and organic light emitting diodes, rely on the properties and performance of thin film polymers.

A fascinating aspect of polymers is the fact that many of their properties change when they are confined to films in the thickness range of nanometers or tens of nanometers. This is largely due to the increasing importance of interfacial interactions and to entropic and enthalpic constraints on the chains in systems. Thus it has become necessary to understand the physics that control the structure, and consequently the properties, of these confined systems.

The work in this thesis involves understanding the behavior of thermally induced transitions in three polymer-based systems confined to thin films: (1) the influence of supercritical CO_2 on the order-disorder transition (ODT) temperature, T_{ODT}, of thin film A-b-B diblock copolymer systems; (2) the influence of particles of nano-scale dimensions on the ODT of thin film A-b-B diblock copolymers, and (3) the glass transition temperature, T_g, of an amorphous linear polymer chain system in which nanoparticles are embedded (a so-called polymer nanocomposite). Both properties exhibit film thickness dependencies, often in ways that are counterintuitive. The goal of the research presented in this dissertation is aimed at the understanding and control of these properties.

A-b-B diblock copolymers exhibit a range of microphase separated symmetries (spheres, cylinders lamellae), above an ODT, depending on the relative volume fractions of the A and B components of the chain.[1-4] Copolymers are particularly attractive for novel applications, ranging from drug delivery to templating of nanostructures. The ODT has been predicted to exhibit some dependence on film thickness and in Chapter 2 we show experimentally, for the first time, that this transition can be shifted by a couple of hundred degrees due largely to chain/substrate interactions. We show, moreover, also for the first time that in the presence of a compressible fluid, supercritical CO_2, the transition in sufficiently thin films can differ considerably from the bulk value. In Chapter 3, it is shown that sterically stabilized metallic nanoparticles can significantly shift the ODT in relation to the pure system. While transitions from one type of symmetry have been predicted and observed, we show the first experimental evidence of the shift in the ODT of a thin film diblock copolymer nanocomposite. Finally, in Chapter 4 we examined how to control the glass transition temperature of homopolymer thin films through the addition of sterically-stabilized nanoparticles. In this instance we carefully selected a

model system in which the interplay between entropic interactions determine the spatial distribution of the nanofillers. This research provides insight on fundamental aspects of the relationship between structure and the glass transition in these thin film systems.

1.2 BACKGROUND AND CONTEXT OF CHAPTERS 2, 3 AND 4

Each of the remaining chapters of this thesis is written in a self-contained manner. The goal of the sections below is to provide background introductory material and context for the research described in the remaining chapters in this dissertation.

1.2.1 Phase Behavior of Diblock Copolymers in the Bulk

As mentioned above, Chapters 2 and 3 demonstrate the possibility of significantly modifying the ODT of an A-b-B diblock copolymer thin film by exposing it to a compressible fluid that is selective to one of the blocks or to sterically stabilized nanoparticles. The goal of this section is to provide an introduction to, and some background material, describing block copolymer bulk and thin film materials. This information will provide a context for the work presented in Chapters 2 and 3.

A-*b*-B diblock copolymers have diverse applications that range from adhesives to optoelectronics. Phase separation below the T_{ODT}[1, 2, 5-11] is accompanied by a minimization of the interfacial area of contact between dissimilar A-rich and B-rich phases. This leads to a reduction of the enthalpy, which is balanced by a reduction of the conformational entropy of the chains, largely connected with stretching, and of the translational entropy. The connectivity between the A and B blocks prohibits large-scale macrophase separation, so phase separation length scales occur on the order of nanometers, determined by the size of the chains. Below the T_{ODT}, spatial arrangement of

the phases exhibits varying symmetries, body centered cubic, hexagonal, lamellar, and bicontinuous gyroid structures (Fig. 1.1a).

Three parameters are used to describe the phase behavior of these materials: the fraction of A monomers, f, that compose the chain and the order parameter χN, where χ is the Flory-Huggins interaction parameter and N is the total degree of polymerization of the chain ($\chi \propto 1/T$, where T is the temperature).[2, 5]

Fig. 1.1b shows the phase diagram, χN versus f, for a generic A-b-B diblock copolymer, showing the regions where the aforementioned morphologies appear. It can be seen that for a symmetric copolymer ($f \sim 0.5$) the order parameter value at the transition is $\chi N=10.5$, and that the corresponding morphology is lamellar. One should note that this value is significantly higher than that observed in binary A/B blends ($\chi N = 2$), as a consequence of the covalent bonding of the A and B blocks.

Depending on the proximity of the copolymer to the transition temperature, there are two different segregation regimes: when $\chi N \sim 10.5$, the copolymer is in the weak segregation limit (SSL), which is characterized by having broad interfaces between the A and B phases[4] . It has also been predicted that the lamellar domain, L, (i.e., for the symmetric diblocks) scales as the radius of gyration,

$$L \propto N^{1/2} \qquad 1.$$

The second, SSL, regime occurs when $\chi N >> 10.5$, and is characterized by very narrow interfacial regions between the phases, compared to the dimensions of the phases.[12, 13] This regime has been investigated thoroughly both theoretically and experimentally. For symmetric diblock copolymers, the interlamellar spacing is

$$L \propto \chi^{1/6} N^{2/3} \qquad 2.$$

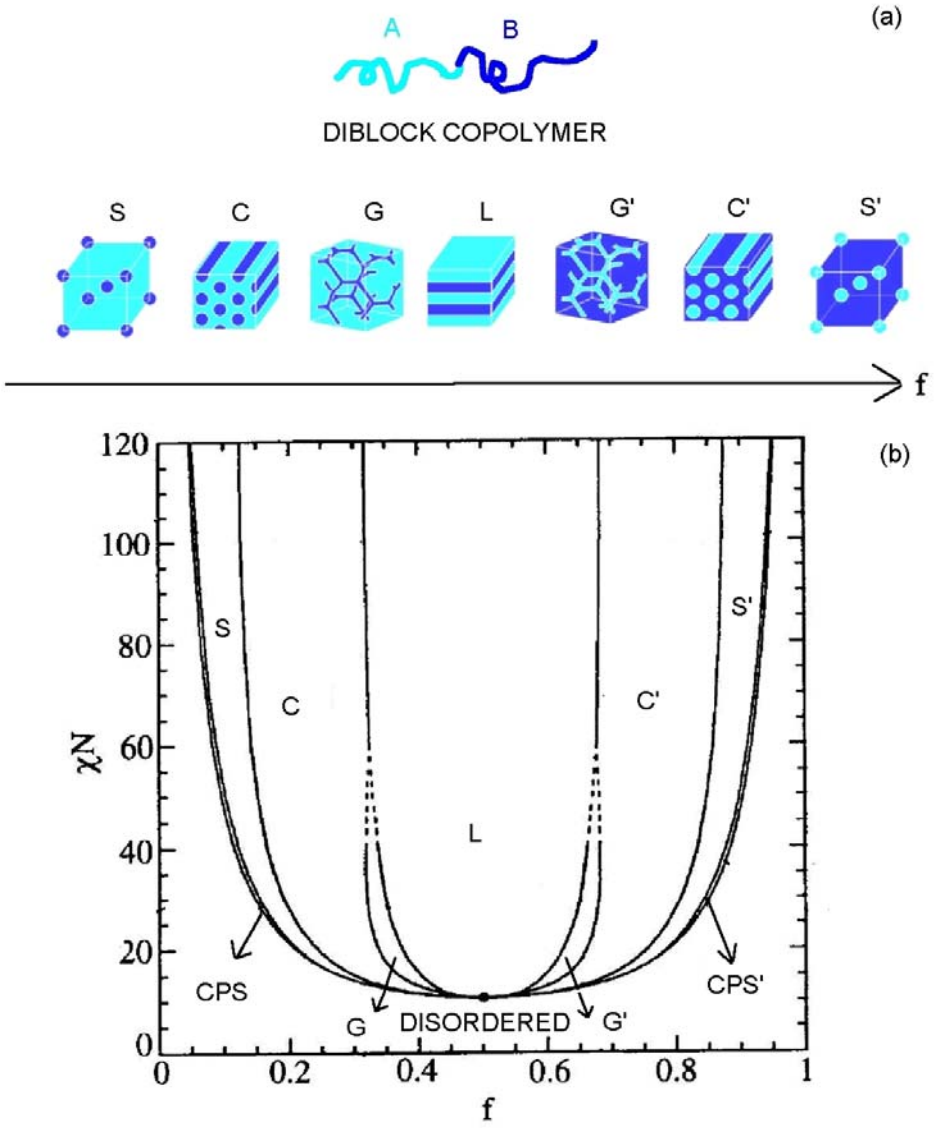

Figure 1.1 (a) Schematic diagram of the morphologies developed by A-b-B diblock copolymers upon phase segregation, as a function of the relative amounts of each block, f: S, spheres; C, cylinders in a hexagonal array; G, gyroid; L, lamellar; CPS, closed-packed spheres. (b) Mean-field phase diagram for a symmetric diblock copolymer, reproduced from The Physics of Block Copolymer[3] with slight modifications.

1.2.2 Phase Behavior of Diblock Copolymer Thin Films: Interfacial Effects

Interfacial interactions, enthalpic and entropic constraints on chain configuration, together with intermolecular forces, both short range (i.e., hydrogen-bonding) and long range (van der Waals), play a critical role toward determining the morphology of polymer thin films. Particularly for the case of diblock copolymer thin films, the interactions between the A, or B, segments and the external interfaces (free surface or substrate) will determine the local segmental concentration profile near the interfaces and will have a profound effect on the resulting morphology of the film. We will focus in the case of lamellar forming, symmetric diblock copolymers (f = 0.5) to facilitate the discussion. Basically two distinct situations may arise depending on whether the diblock is above, or below its T_{ODT}.

When the film is below its T_{ODT}, the polymer is in an ordered state, that is, it undergoes microphase separation. Due to the block connectivity, the composition profile becomes either a sinusoidal-like pattern (in the WSL), or a series of alternating pure domains of each segment (in the SSL).

In typical situations, the lamellae tend to orient parallel to the plane of the substrate due to the preferential attraction that the monomers have towards each of the two interfaces.[1, 6-10, 14, 15] The interface potential that gives rise to this type of composition profile is a periodic function of film thickness, h (Fig. 1.2a). The locations of the minima in the free energy denote the stable film thicknesses. This means that the free surface of a sufficiently thin film of thickness h, supported by a substrate, will remain flat, stable, if h corresponds to the location of any minima in the free energy function.

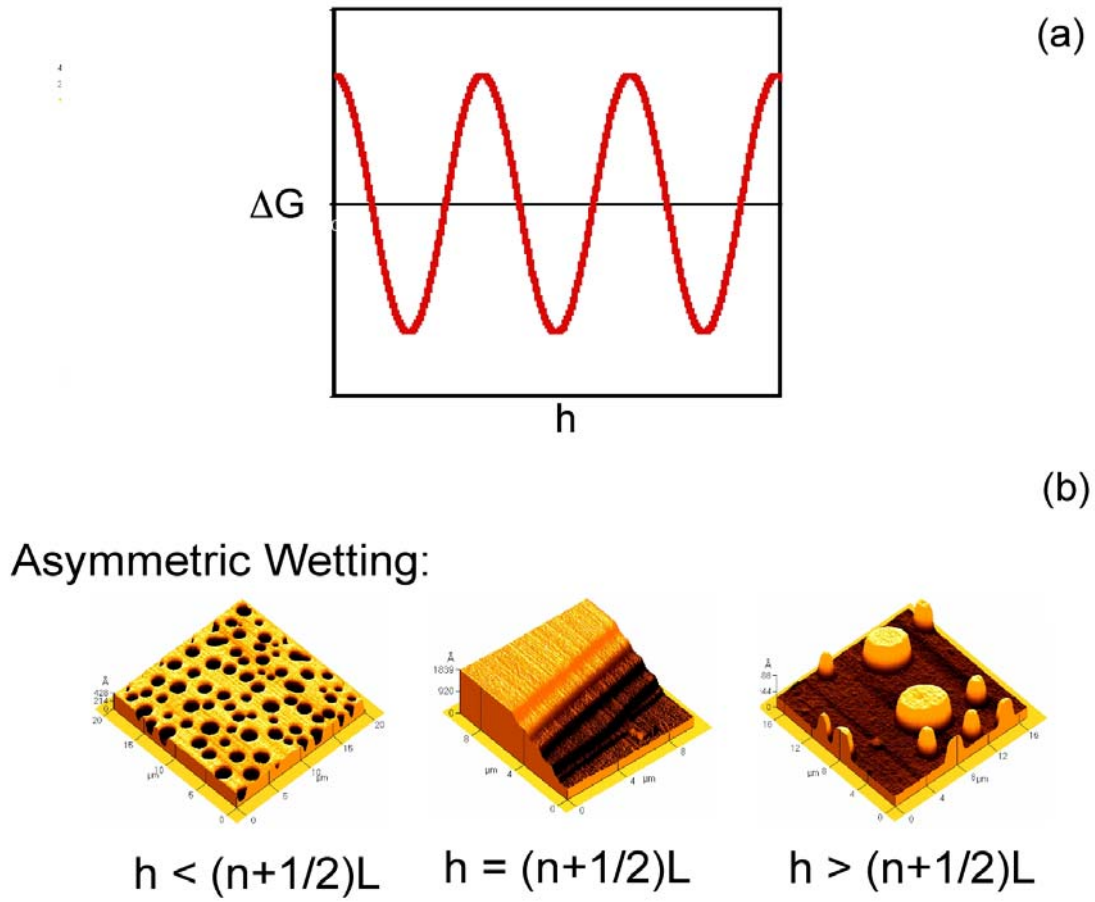

Figure 1.2 (a) A sketch of the effective interface potential as a function of film thickness for a diblock copolymer below its T_{ODT}. (b) Representative topographies of ordered PS-b-PMMA block copolymer films forming holes,[6] smooth films, or islands depending on the commensurability of the initial film thickness with the position of the minima in the interface potential.

If the same component is attracted to the free surface and to the substrate (symmetric wetting case, represented in figure 1.3a), the free energy minima are located at film thicknesses h = nL, where n is an integer. For the asymmetric wetting case (different component at the free surface and at the substrate, shown in figure 1.3b)) the minima are located at film thicknesses h = (n + 1/2)L.

For films whose thicknesses do not meet the appropriate stability criteria, associated with a minimum, a discontinuous layer of thickness L develops at the free surface (Fig. 1.2b). That is, the films try to minimize the free energy of the system by forming structures with a height that coincides with the position of the nearest minimum.

The topography is thus composed of "islands" or "holes," depending on how far the film thickness deviates, δh, from the appropriate stability criterion. The "islands" and "holes" account for the excess thickness, δh, and are indicative of self-organization, or order, within the film.

Destabilization of films above the T_{ODT} results in a hierarchy of transient and stable topographies. The mechanism that engenders each type of topography is correlated to the curvature of the interface potential. Specifically, above the ODT temperature, the effective interface potential becomes an oscillatory function that dampens with increasing film thickness (Fig. 1.4a). Films with thickness in the range where the potential has negative curvature destabilize through a spinodal process. On the other hand, films with thickness values in the range where the potential exhibits positive curvature destabilize through nucleation of holes. Once again, the minima correspond to stable films with a smooth topography. It is important to note that the thickness value where the global minimum of the potential lies is not only stable, but is formed by a brush of phase segregated material of thickness L or L/2 (depending on the wetting symmetry of the system). The brush formation is ensued by the preferential affinity of the blocks to the

interfaces and results in short-range order. Thus, any excess material located on top of this brush layer will be disordered and the topographies formed will not be commensurate with the lamellar period of the diblock copolymer (Fig 1.4b).

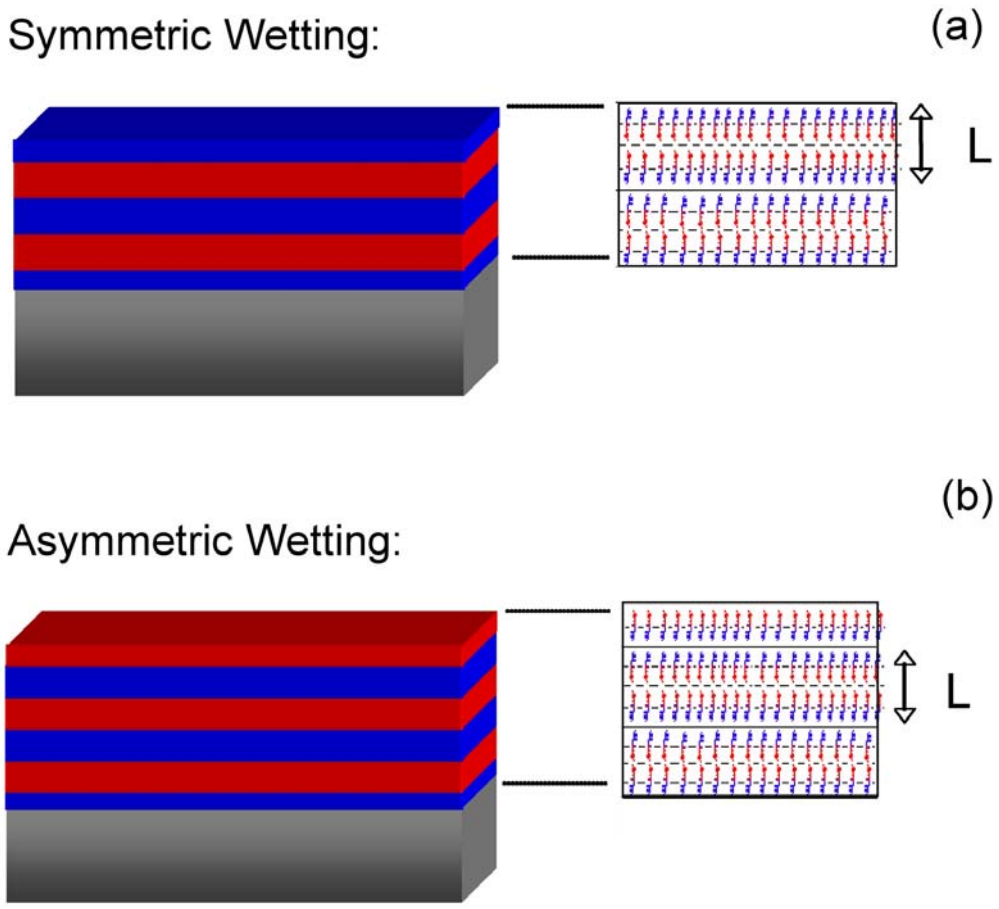

Figure 1.3 Schematic representation of the lamellar structures formed upon phase segregation of a symmetric diblock copolymer thin film supported by a substrate for: (a) symmetric wetting case (b) asymmetric wetting case.

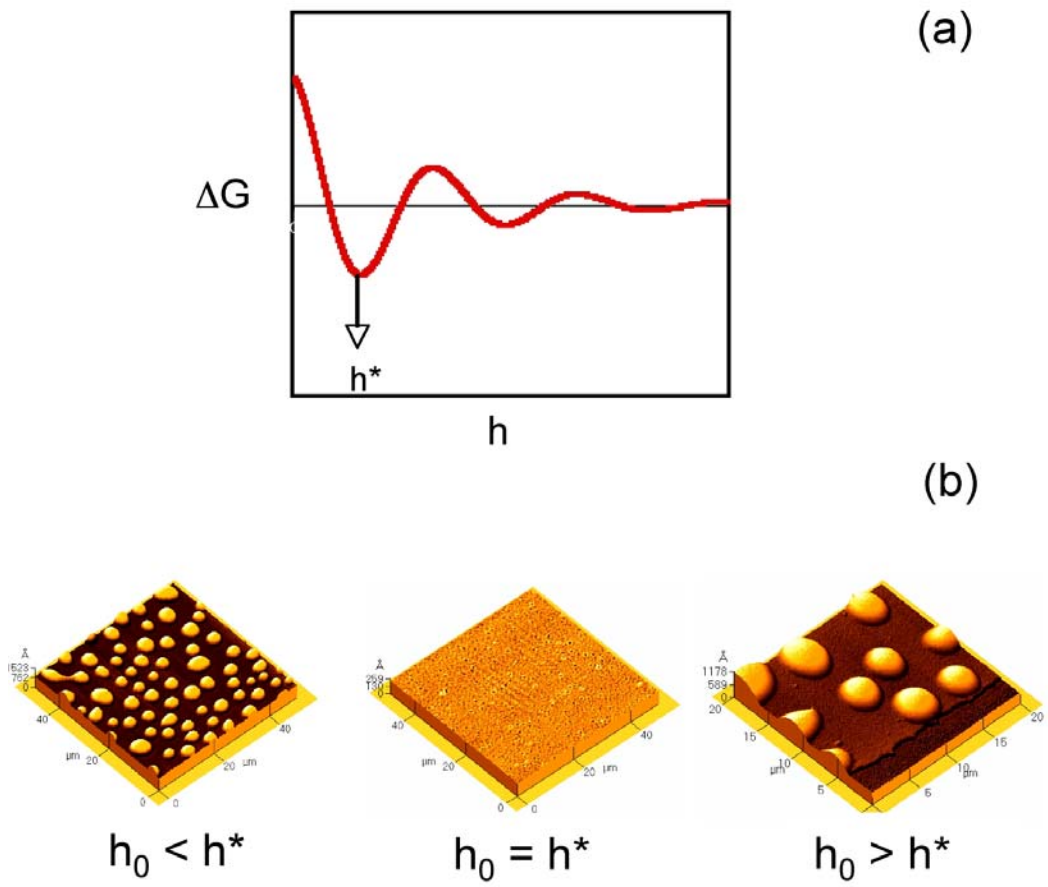

Figure 1.4 (a) Schematic drawing of the effective interface potential as a function of film thickness for a diblock copolymer above its T_{ODT}. (b) Representative topographies of phase mixed, PS-b-PMMA diblock copolymer films forming droplets on a substrate, a smooth film, or droplets on a brush, depending on their thickness in relation to the minimum in the interface potential.

1.2.3 Diblock Copolymer/Nanoparticle Nanocomposites

In Chapter 3 of this dissertation, we discuss the effects of the addition of selective metallic nanoparticles of varying size on the order-disorder transition of diblock copolymer thin films supported by silicon nitride substrates. Below we provide an introduction and background describing the phase behavior of block copolymer-nanoparticle systems.

Recently, there has been increasing interest in exploiting the self-assembling capabilities of diblock copolymer to fabricate highly-ordered, organic/inorganic hybrid materials by mixing the polymeric matrix with nanoscopic inorganic particles. The periodic nanostructures thus obtained are expected to lead to significant changes in the properties of the material, as compared to those of the pristine polymeric matrix. A thorough understanding of the enthalpic and entropic effects that result in a given structure is consequently key to be able to elucidate the structure-property relationships in these hybrid systems.

Simulations show that particles with neutral interactions with the A and B phases, if sufficiently large compared to the domain dimensions, will form a separate ordered phase. This is largely due to entropic constraints imposed on the copolymer chains associated with incorporating the large particles within a domain. If the particles are sufficiently small, they tend to segregate preferentially toward the interfacial regions between the A and B phases of the copolymers[16, 17] (Fig 1.5a); the effect is to reduce the degree of incompatibility between the phases and this could influence the temperature, T_{ODT}, at which the transition occurs.

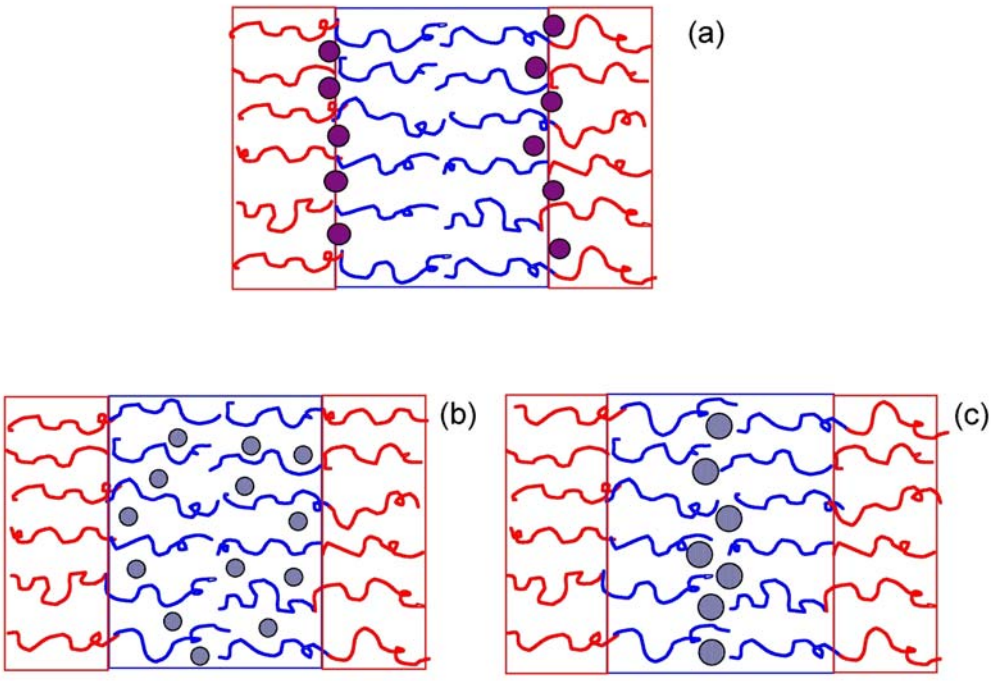

Figure 1.5 Schematic of the distribution of nanoparticles within a block copolymer for (a) small filler particles with neutral interactions towards both blocks, (b) small fillers with preferential interactions with one of the blocks and, (c) large fillers with preferential interactions for one block.

On the other hand, if the particles are compatible with one phase, for example the A-phase, they will preferentially segregate toward that phase, provided they are sufficiently small.[18, 19] The particles are reasonably distributed throughout a single domain to maximize the translational entropy (Fig 1.5b).

As the particles increase in size, the stretching energy (conformational entropy) of the chains increases. Consequently, larger particles will segregate primarily to the center of the domains, to reduce the stretching (Fig. 1.5c). For the same volume fraction, these smaller particles can have the effect of swelling the domains more than the larger particles. Homopolymer chains have been shown to behave in a manner similar to the nanoparticles in that small chains are distributed throughout the domain and larger chains are concentrated toward the center of the domains.[20, 21]

In addition to swelling the domains of the copolymers, nanoparticles have been shown, experimentally[22] and theoretically[19], to induce transitions from one ordered phase to another.

The effects of confinement and interfacial interactions on the structure of block copolymer/nanoparticles systems have been scarcely studied. However, Lee et al.[23] showed that confinement of a symmetric A-B diblock copolymer between two A-like hard surfaces can result in the segregation of the nanoparticles to the interfaces. The particles are pushed to the interface to avoid the conformational entropy loss of the chains incurred by having to accommodate these inclusions in the 'bulk' of the film. Even more, if the volume fraction of nanoparticles is sufficiently high, the chemical nature of the interfaces is effectively modified, resulting in a reorientation of the microdomains to form lamellae that lie perpendicular to the interfaces.

1.2.4 Glass Transition of Polymer Thin Films

In recent years, numerous studies have shown that the T_g of thin polymer films exhibits a thickness dependence.[24-26] This behavior is thought to arise from an interplay between confinement effects and interfacial interactions within the film. By confinement effects it is understood that polymer chains experience changes in their configurational freedom when they lie close to an interface. More specifically, the configurational entropy of chains that lie close to a substrate is usually restricted compared to that of 'bulk' chains, while a gain in this entropy is expected for chains that are exposed to a free surface. On the other hand, interfacial interactions can arise when chain structure makes it possible for specific interactions to take place between substrate and polymer like, for example, hydrogen bonding.

In fact, it has been consistently observed that polymers that have specific interactions with a substrate (i.e. PMMA /Si-SiOx, PVP/Si-SiOx)[25] present an increase in their T_g with decreasing film thickness, whereas polymers that lack such interactions (for example PS/Si-SiOx)[26] actually decrease their T_g upon a decrease in thickness.

Several models have been proposed to understand this behavior, for example, Keddie et al.[25, 26] propose that the free surface of a thin film has a liquid-like behavior (Fig. 1.6a). As the film thickness decreases, the upper layer has more influence on the overall behavior of the films.

$$T_g = T_g(\infty)[1-(A/h)^{\delta}] \qquad 3.$$

Where $T_g(\infty)$ is the glass transition temperature at large thickness h, d indicates the degree to which T_g decreases with decreasing film thickness, and A is a length scale.

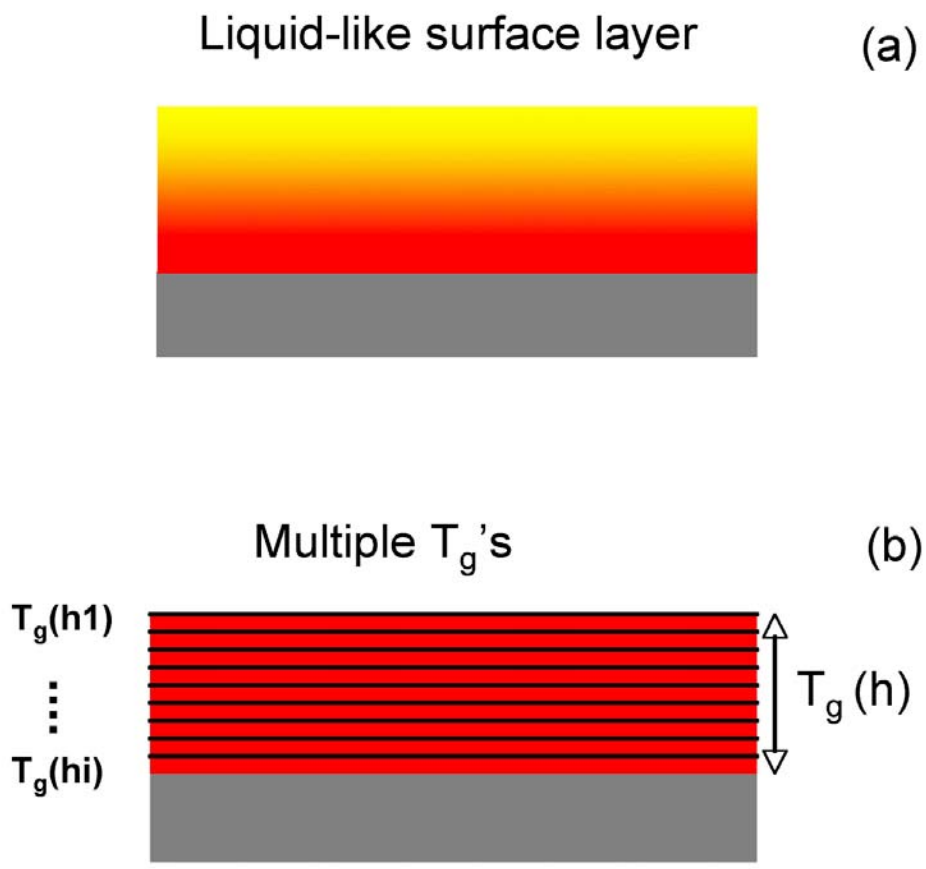

Figure 1.6 Schematic representations of models designed to describe the thickness dependence of the glass transition in polymers confined to a thin film geometry. (a) Liquid-like surface layer model proposed by Keddie et al.[25, 26] (b) Multiple T_g model proposed by Kim et al.[24]

Kim et al.[24] proposed a model in which the polymer film is viewed as a series of films stacked on top of each other, each with a different T_g (Fig. 1.6b). Here the top layer has the lowest T_g and as the layers go deeper into the film, the T_g increases.

$$T_g(h) = T_{g,bulk}\frac{h}{\sigma + h} \qquad 4.$$

where σ is a measure of the rate at which the glass transition temperature decreases with decreasing thickness, h.

McCoy and Curro[27] devised a model based on the density of the film, whereby a film with a lower density than that of the bulk has a lower T_g (Fig. 1.7). This implies that chain packing determines the sign of the change of T_g, ΔT_g.

$$\Delta T_g = \frac{1}{\kappa}\frac{dT_g}{dP}\frac{2\Gamma(H)}{H\rho_{bulk}} \qquad 5.$$

$$\text{where} \quad \Gamma(H) = \frac{1}{2}\int_0^H \left[\rho(z) - \rho_{bulk}\right].$$

Here, κ is the bulk modulus, and H is a segmental confinement length.

The final model we will discuss is based on the concept of dynamic heterogeneity within the film, given by Long and Lequeux[28]. They propose that the dynamics within a polymer are a result of the coexistence of fast and slow domains within the material. This heterogeneity arises from local thermal fluctuations of the density, which in turn affects dynamics in a non-linear fashion (Fig. 1.8). The glass transition is thought to be associated with the percolation of the slow domains.

$$\frac{T_g(h) - T_{g,bulk}}{T_{g,bulk}} \approx \frac{-2.6}{N_c^{(1/2-1/(3r))}}\frac{a}{h}\log\left(\frac{h}{2\xi}\right) \qquad 6.$$

where ν is a critical exponent for percolation in three dimensions and ξ is a correlation length. Since the percolation threshold is lower in two dimensions than in three dimensions, the T_g of a freely standing film should be lower than that of the bulk polymer.

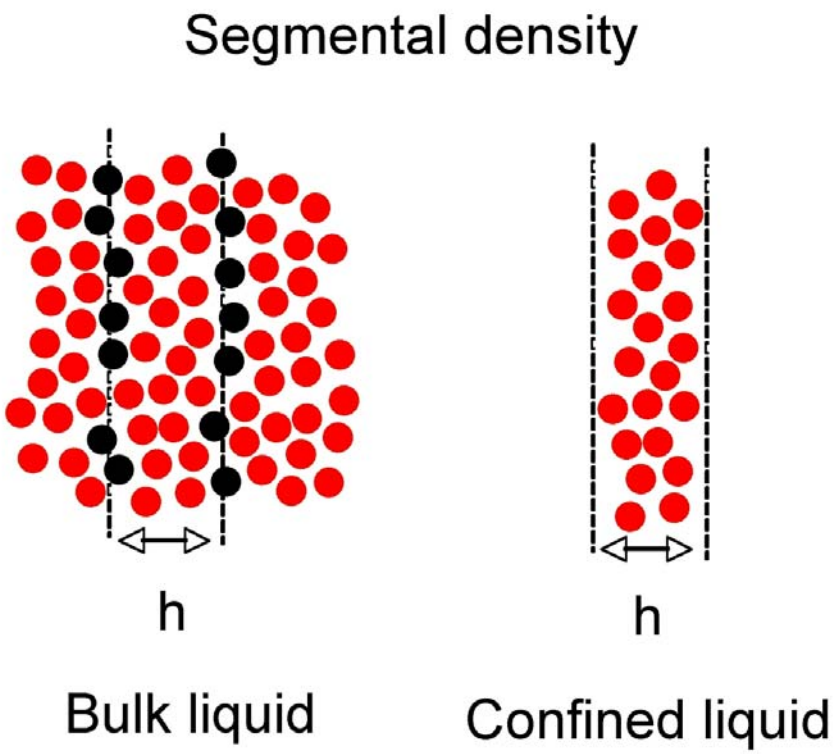

Figure 1.7 Schematic of the changes in the segmental density profile of a liquid confined to a thin film geometry, which are used to explain the thickness dependence of T_g. The diagram is an adaptation from McCoy and Curro.[27]

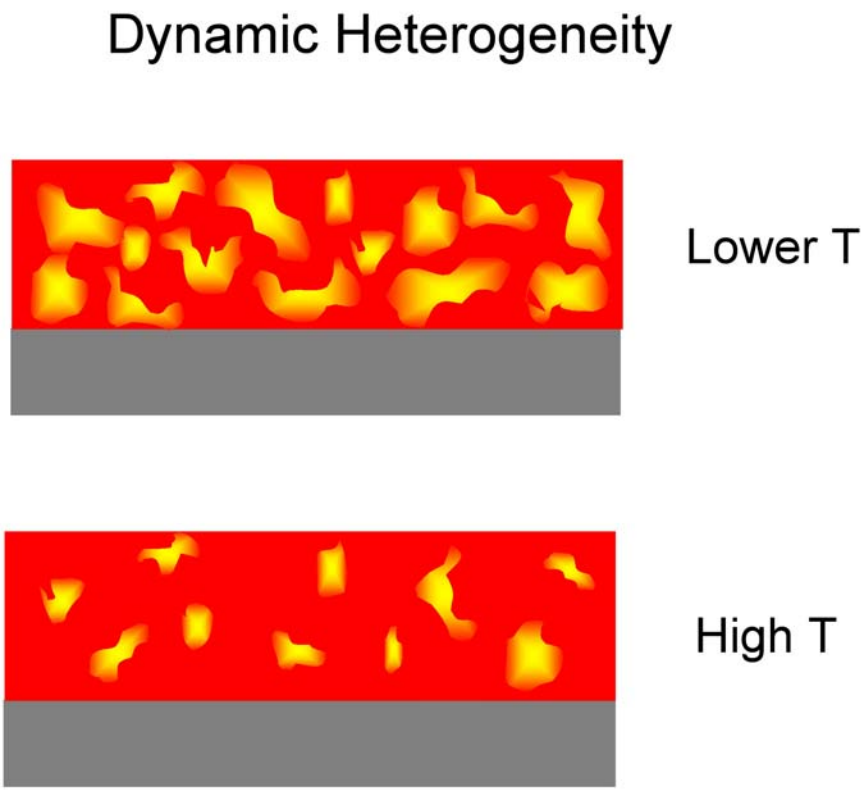

Figure 1.8 Illustration of the coexistence of regions of fast (red) and slow (yellow) dynamics which give rise to the glass transition of polymers upon percolation.[28]

On the contrary, a strongly interacting wall should give rise to a larger fraction of slow domains in a film, which should lead to an increase in T_g, with respect to that of the bulk.

While most studies on thin films have focused on the T_g vs. h behavior of homopolymer systems, some experiments with blends have been carried out. It is worth mentioning that the aforementioned models have been successfully applied to model experimental results of thin polymer mixtures. Pham et al.[29, 30] studied a miscible blend of TMPC/PS on Si/SiOx substrates. This is an asymmetrically wetting substrate, with TMPC adsorbing to the substrate, while PS enriches the free surface due to a lower surface energy, γ. The authors show that pure TMPC films show a positive ΔTg with decreasing thickness, consistent with the notion of highly interacting polymer-substrate behavior. However, films having a composition of 70-30 TMPC:PS show the opposite behavior, suggesting that the higher mobility in the surface (where there is a measured composition of ~75% PS) dominates the T_g behavior. It is clear now that both confinement and surface interactions play a decisive role in the behavior of T_g vs h of thin polymer films.

1.2.5 Glass Transition in Polymer Nanocomposites

Bulk and thin film polymer nanocomposites have gained much attention recently due to the enhanced properties[31-34] endowed by novel nanomaterials, like inorganic nanoparticles, nanoclays, carbon nanotubes, etc. In comparison to traditional microscopic fillers, the nanoscopic dimensions of the dispersed particles can lead to a greater effective surface area of polymer segments in contact with the filler at a given particle volume fraction. Moreover, chain confinement and polymer bridging between particles are relatively commonplace in polymer nanocomposites due to the fact that

interparticle separation distances become comparable to the average size of the polymer chain at low particle volume fractions. While much has yet to be learned about these systems, it is expected that these factors play a significant role in the resulting properties of the nanocomposites.

The importance of interfacial interactions and confinement effects in the properties of these systems has naturally led researchers to make connections between the behavior of polymer nanocomposites and polymer thin film systems.[31] The dynamic percolation model described above[28] suggests that the presence of particles should affect the fraction of slow domains in these systems, and consequently their glass transition. Generally, one would expect an increase in the T_g of the polymer upon addition of strongly interacting particles, while a decrease in the T_g should be favored when the particles surfaces are neutral or repulsive.[35-38]

The dependence of the T_g of polymer nanocomposites on the polymer-particle interactions has been mostly studied for hard-sphere particle/polymer mixtures. In practice, `soft´ particles, obtained by the grafting of polymer chains on the particle surface, are often used to counteract the strong attractive interactions between inorganic cores that can lead to their aggregation. In Chapter 4, we examine the glass transition of athermal thin film mixtures of polymer-coated metallic nanoparticles embedded within a chemically-identical homopolymer film. It is seen that control of the location of nanoparticles within the film can be obtained by tailoring nanoparticle size and brush characteristics. Such control over the structure of the nanocomposite is of great importance to gain a deeper understanding of the glass transition behavior in these thin film nanocomposite systems.

1.3 REFERENCES

1. Anastasiadis, S. H.; Russell, T. P.; Satija, S. K.; Majkrzak, C. F. *Physical Review Letters* **1989,** 62, (16), 1852-1855.

2. Bates, F. S.; Fredrickson, G. H. *Annual Review of Physical Chemistry* **1990,** 41, 525-557.

3. Hamley, I. W., *The physics of block copolymers*. Oxford University Press: Oxford, 1998.

4. Leibler, L. *Macromolecules* **1980,** 13, (6), 1602-1617.

5. Fredrickson, G. H. *Macromolecules* **1987,** 20, (10), 2535-2542.

6. Green, P. F. *Journal of Polymer Science Part B-Polymer Physics* **2003,** 41, (19), 2219-2235.

7. Limary, R.; Green, P. F.; Shull, K. R. *European Physical Journal E* **2002,** 8, (2), 103-110.

8. Mansky, P.; Tsui, O. K. C.; Russell, T. P.; Gallot, Y. *Macromolecules* **1999,** 32, (15), 4832-4837.

9. Menelle, A.; Russell, T. P.; Anastasiadis, S. H.; Satija, S. K.; Majkrzak, C. F. *Physical Review Letters* **1992,** 68, (1), 67-70.

10. Shull, K. R. *Macromolecules* **1992,** 25, (8), 2122-2133.

11. Smith, A. P.; Douglas, J. F.; Meredith, J. C.; Amis, E. J.; Karim, A. *Physical Review Letters* **2001,** 8701, (1), -.

12. Helfand, E. *Macromolecules* **1975,** 8, (4), 552-556.

13. Helfand, E.; Wasserman, Z. R. *Macromolecules* **1976,** 9, (6), 879-888.

14. Orso, K. A.; Green, P. F. *Macromolecules* **1999,** 32, (4), 1087-1092.

15. Smith, M. D.; Green, P. F.; Saunders, R. *Macromolecules* **1999,** 32, (25), 8392-8398.

16. Schultz, A. J.; Hall, C. K.; Genzer, J. *Macromolecules* **2005,** 38, (7), 3007-3016.

17. Wang, Q.; Nealey, P. F.; de Pablo, J. J. *Journal of Chemical Physics* **2003,** 118, (24), 11278-11285.

18. Huh, J.; Ginzburg, V. V.; Balazs, A. C. *Macromolecules* **2000,** 33, (21), 8085-8096.

19. Thompson, R. B.; Ginzburg, V. V.; Matsen, M. W.; Balazs, A. C. *Science* **2001,** 292, (5526), 2469-2472.

20. Matsen, M. W. *Macromolecules* **1995,** 28, (17), 5765-5773.

21. Likhtman, A. E.; Semenov, A. N. *Macromolecules* **1997,** 30, (23), 7273-7278.

22. Kim, B. J.; Chiu, J. J.; Yi, G. R.; Pine, D. J.; Kramer, E. J. *Advanced Materials* **2005,** 17, (21), 2618-+.

23. Lee, J. Y.; Shou, Z. Y.; Balazs, A. C. *Macromolecules* **2003,** 36, (20), 7730-7739.

24. Kim, J. H.; Jang, J.; Zin, W. C. *Langmuir* **2001,** 17, (9), 2703-2710.

25. Keddie, J. L.; Jones, R. A. L.; Cory, R. A. *Europhysics Letters* **1994,** 27, (1), 59-64.

26. Keddie, J. L.; Jones, R. A. L.; Cory, R. A. *Faraday Discussions* **1994**, (98), 219-230.

27. McCoy, J. D.; Curro, J. G. *Journal of Chemical Physics* **2002,** 116, (21), 9154-9157.

28. Long, D.; Lequeux, F. *European Physical Journal E* **2001,** 4, (3), 371-387.

29. Pham, J. Q.; Green, P. F. *Macromolecules* **2003,** 36, (5), 1665-1669.

30. Pham, J. Q.; Green, P. F. *Journal of Chemical Physics* **2002,** 116, (13), 5801-5806.

31. Bansal, A.; Yang, H. C.; Li, C. Z.; Cho, K. W.; Benicewicz, B. C.; Kumar, S. K.; Schadler, L. S. *Nature Materials* **2005,** 4, (9), 693-698.

32. Krishnamoorti, R.; Giannelis, E. P. *Macromolecules* **1997,** 30, (14), 4097-4102.

33. Mackay, M. E.; Tuteja, A.; Duxbury, P. M.; Hawker, C. J.; Van Horn, B.; Guan, Z. B.; Chen, G. H.; Krishnan, R. S. *Science* **2006,** 311, (5768), 1740-1743.

34. Tsagaropoulos, G.; Eisenberg, A. *Macromolecules* **1995,** 28, (18), 6067-6077.

35. Smith, G. D.; Bedrov, D.; Li, L. W.; Byutner, O. *Journal of Chemical Physics* **2002,** 117, (20), 9478-9489.

36. Starr, F. W.; Schroder, T. B.; Glotzer, S. C. *Physical Review E* **2001,** 6402, (2), -.

37. Starr, F. W.; Schroder, T. B.; Glotzer, S. C. *Macromolecules* **2002,** 35, (11), 4481-4492.

38. Pryamitsyn, V.; Ganesan, V. *Macromolecules* **2006,** 39, (2), 844-856.

Chapter 2: The Ordering Transition of Block Copolymer Films

2.1 INTRODUCTION

A distinctive feature of diblock copolymers is their ability to self-assemble into periodic structures with nanometer dimensions below an order-disorder transition, ODT.[1-6] The driving force for this process is the minimization of unfavorable contacts between the constituent blocks of the chain, at the cost of conformational and translational entropy. This self-assembling capability makes diblock copolymers useful for a wide range of applications involving, for example, templating periodic patterns for microelectronics, synthesis of porous materials, or patterning in lithography.[7-12]

In some of these applications, the block copolymer is confined to a thin film, usually supported by a solid substrate. Under these conditions, interactions of the block constituents with the interfaces can have a profound impact on the film topography and morphology,[4] as discussed in Chapter 1. Precise control of the desired morphological structure and large-scale order is, however, a challenging endeavor. It is therefore desirable to devise processing schemes which allow the control of structure formation in this type of systems by modifying interfacial interactions. One common approach to achieve this goal is processing the films under saturated solvent vapor environments which have some affinity towards one of the blocks, and which also allow the process to be carried out at low temperatures. Along the same lines, the use of supercritical fluids has become perhaps a more attractive alternative, due to the tunability of its solvent properties, which permits manipulation of interfacial interactions with small adjustments in pressure or temperature.

Most polymers are subject to swelling and plasticization by supercritical CO_2, which can cause depressions in their T_g of several tens of degrees. With respect to the sorption and swelling, it has been observed that CO_2 can be absorbed by as much as 20 wt. %, depending on the specific polymer. A key factor that determines the amount of CO_2 absorbed by a polymer is the type of short range interactions that might take place between the compressed gas and the monomers in the chain. For example, Zhang et al.[13] observed that poly(methylmethacrylate) (PMMA) absorbs twice as much CO_2 as poly(styrene) (PS), due to the attractive interactions between the carbonyl groups of both PMMA and the CO_2 . There is no such type of interaction in the PS/CO_2 system thus resulting in lower sorption levels.

Remarkable differences have been observed in the phase behavior of polymer blends and diblock copolymers in the presence of CO_2. In the case of diblocks with lower disorder-order transition temperature (LDOT) and lower critical solution temperature (LCST)-type blends, it has been observed that the transition temperature can be shifted tens of degrees upon sorption of small amounts of CO_2[14-18] (Fig. 2.1b).

The cause of this behavior is that the CO_2-polymer system becomes highly compressible in comparison to the melt. Further, due to preferential sorption of CO_2 into one of the polymers in the blend, the difference in compressibility increases with increasing CO_2 content. This drives the blend to phase separate.

On the other hand, diblock copolymers with an upper order-disorder transition temperature (UODT) and upper critical solution temperature (UCST)-type blends have been shown to exhibit a decrease of a few degrees in their critical solution temperature[14-18] (Fig. 2.1a). The tendency of the copolymer toward phase mixing in CO_2 is due to a lowering of the interfacial tension between the A and B-blocks (or homopolymer chains) and to the screening of unfavorable enthalpic interactions between the A-B blocks or

blend components. This behavior is not uncommon with supercritical solvents or with slightly selective organic solvents

In the present study, we examine the influence of a SiO_x/Si substrate on the ordering of thin film symmetric PS-*b*-PMMA copolymers with thicknesses less than twice the lamellar period (h<2L) in (1) vacuum environments at 170°C and (2) in compressed CO_2 environments at 170°C. We show that while in vacuum (or air) bulk copolymer mixtures may be phase mixed, the substrate induces significant order in these films, shifting the bulk ODT by $\left[(\chi N)_{bulk-ODT} - (\chi N)_{film-ODT}\right]/(\chi N)_{blk-ODT} \approx 0.24$, which corresponds to a shift of over 100 degrees. In compressed CO_2, the ODT is shifted further, at least by $\left[(\chi N)_{bulk-ODT} - (\chi N)_{film-ODT}\right]/(\chi N)_{blk-ODT} > 0.29$, not lower!

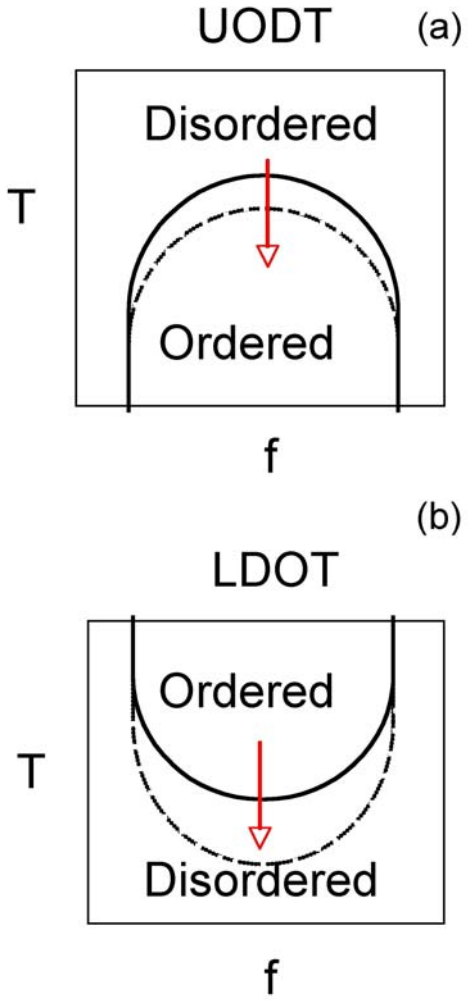

Figure 2.1 Schematic illustrating the effects of CO_2 on the phase diagram of a block copolymer. The solid curves represent the diagram under air/vacuum environments whereas the dashed curves represent the diagram under $scCO_2$ conditions. (a) CO_2 lowers the upper order –disorder transition (UODT) temperature favoring mixing. (b) CO_2 reduces the lower disorder-order transition (LDOT) temperature inducing phase segregation.

2.2 EXPERIMENTAL SECTION

Mixtures of symmetric poly(styrene-b-methyl methacrylate) (PS-*b*-PMMA) of two different molecular weights, M_n = 20,500 g/mol (N=201) and 65,500 g/mol (N = 650), were blended in different proportions to prepare samples of number average degrees of polymerization, from N=201 to 650. The value of the PS-PMMA Flory-Huggins interaction parameter, χ, at this temperature is 0.0368[19]. Since *N* in this study ranged from 201 to 650, the values of χN for the samples ranged from 7.4 to 25.8 at 170°C. The molecular weight distributions of these polymers were narrow, M_w/M_n = 1.14 and 1.06 for the long and short copolymers, respectively. These copolymers are polymer standards purchased from Polysciences, Inc. The mixtures were dissolved in toluene and spin coated onto polished silicon wafers. A native oxide layer of approximately 1.5 nm resided on the Si substrate, as measured by ellipsometry. Different thicknesses of copolymer films were spin coated for each mixture: h = 10-40nm (i.e. all samples are of thickness h < 2L). A series of films were scored at the center and then annealed under vacuum at 170°C for approximately 16 h. This provided more than sufficient time for the topographies to develop. Generally, techniques such as transmission electron microscopy or scattering measurements are reliably used to demonstrate order or disorder in these systems. However since the existence of the topography is indicative of order (phase segregation) then analysis involving scanning force microscopy (SFM) is a viable alternative.

The samples were subsequently quenched to room temperature after processing and then scanned using scanning force microscopy (SFM) in the contact mode. A second series of samples of the same thickness range was processed under a CO_2 atmosphere (Matheson 99.9999% purity) at 170°C, 110°C and 60°C, and a pressure of 145 bar,

enclosed within a fixed volume, high-pressure cell. After a processing period of 24 h, the cell was cooled to ~ 25°C, depressurized to ambient pressure at a rate of one bar per second, and then scanned using contact mode scanning force microscopy.

2.3 RESULTS AND DISCUSSION

2.3.1 Diblock copolymer in vacuum at 170°C

A series of samples were annealed under vacuum conditions at a temperature of 170°C, which corresponds to the bulk order disorder transition of a sample with N = 292. In vacuum (or air), PS is preferentially attracted to the free surface because of its lower surface tension at this temperature, whereas PMMA is preferentially attracted to the SiO_x/Si substrate. A common feature of all the films is that a "brush" layer of copolymer is formed at the SiO_x/Si substrate after annealing.[1, 4, 6, 20-24] The brush layer represents the self-organization of a single layer of copolymer chains (Figure 2.2a); hence its thickness is L/2 (Figure 2.2b), where L is the interlamellar spacing. Droplets reside on this brush layer and the dimensions of the droplets bear no relation to L. The schematic in part (c) of this Figure shows the organization of chains in the vicinity of the substrate; the chains in the droplet lack the order of the chains in the brush.

Previous studies of thin films of the N=200 (M_w=20,500 g/mol) copolymer sample were conducted by Limary and Green[24-26]. This sample is disordered in the bulk and in thin films the brush layer of thickness h=L/2=7 nm resides on the SiO_x/Si substrate. Beyond this layer, the sample is disordered as droplets reside on its surface. The effective interface potential (free energy of interaction per unit area) for this sample is characterized by a damped oscillatory profile with a minimum at h=L/2 corresponding to a stable film thickness (asymmetric wetting)[26].

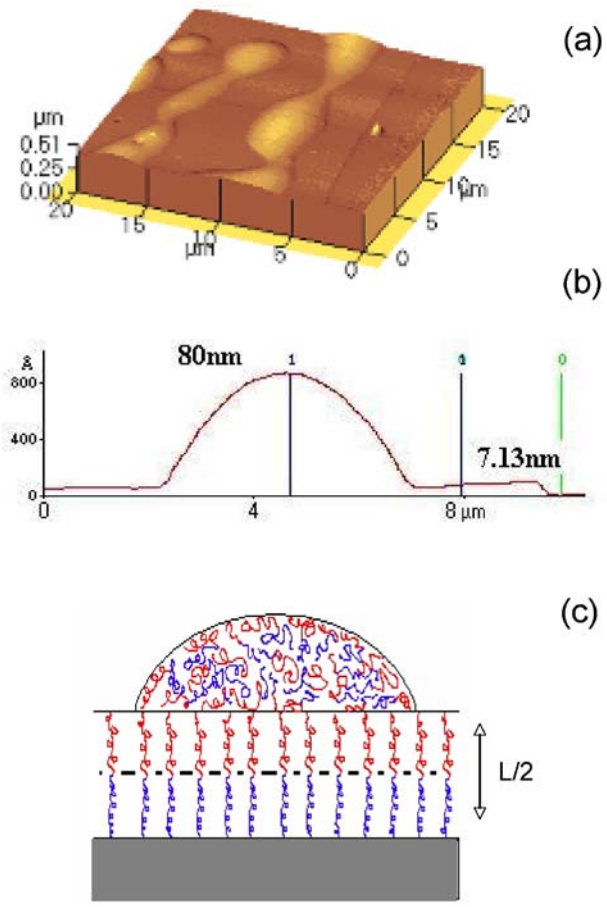

Figure 2.2 An SFM image of a 20 nm film of N = 208 annealed at 170°C is shown in part (a). Droplets reside on the brush layer of thickness L/2 = 7.14 nm, as indicated by the accompanying line scan in part (b). The sizes of the droplets bear no relation to L. Shown in part (c) is a schematic of the local organization of the chains where the droplet is on contact with the brush layer, with the brush layer in contact with the substrate.

This layer is one half of the interlamellar spacing because the PS component is preferentially attracted to the free surface and PMMA to the substrate. This is the thickness of the brush layer. The topography is determined by curvature of the effective interface potential at the relevant film thickness. When the curvature of the profile is negative, spinodal patterns were observed, otherwise holes develop. It was shown that the topographies of films thicker than L/2 but less than approximately 5L/2 were characterized by transient holes or spinodal patterns. These topographies eventually evolved into droplets at sufficiently long times. Thicker films remain kinetically stable.

The topography of the film illustrated in Figure 2.2 is readily rationalized with a similar picture involving the effective interface potential. The brush layer would correspond to a lamellar thickness of L/2 and the transient topographies observed in the figure would be associated with the shape of the effective interface potential at the relevant film thickness. In fact, films of N equal to and less than 210 exhibited similar behavior, formation of a single brush layer on which droplets resided. The observations are rationalized in terms of a single minimum in the damped oscillatory profile, as was done by Limary et al.[24] for the copolymer of N = 201 (M_n = 20,500 g/mol.).

Samples with degrees of polymerization of N > 216 were ordered throughout; terraces (islands or holes) of height L resided on the brush layer of thickness L/2 in each case (Figure 2.3a). Figure 2.3b shows a typical line scan of holes in a sample of initial thickness h = 20 nm (N = 216). There the brush layer is of thickness h_0 = 8.4 nm and the second layer of height L = 18 nm. These results indicate that this sample is ordered throughout the thickness range of up to 2L (Droplets reside on the surfaces of films with thicknesses h > 2L or thicker), as illustrated in Figure 2.3c.

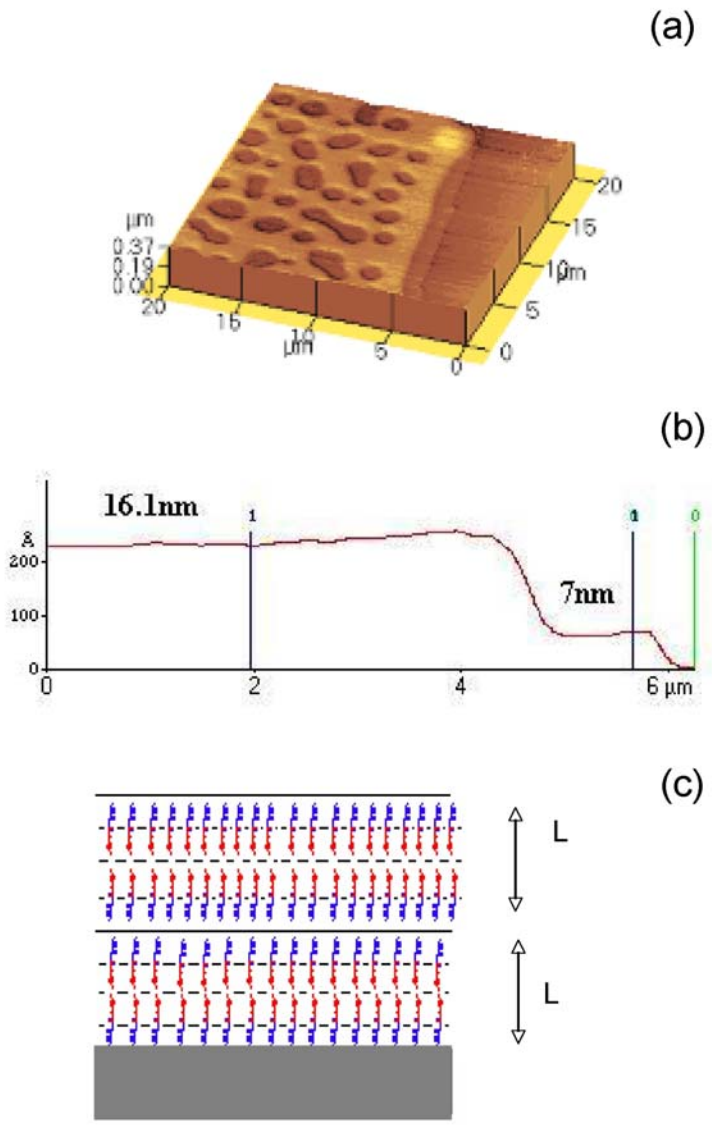

Figure 2.3 An SFM image of the topography of a sample of N = 216 (χN = 7.94) (N = 208) with thickness h = 20 nm annealed at 170°C is shown in part (a). The line scan, part (b), indicates that the second layer is ordered and of thickness twice that of the brush layer. (c) Schematic representation of the ordered lamellar structures present in this phase segregated film.

An estimate of an upper bound of the shift of the ODT associated with the ordering of the second layer due to the influence of the substrate may be obtained from our data. For the sample with N = 216, the bulk ODT would occur at a temperature of – 84°C. The film is ordered over the thickness range of h < 2L at 170°C, indicating that the ODT is shifted by at least a temperature of approximately 254 °C. Alternatively, the shift may be viewed as

$$\left[(\chi N)_{bulk-ODT} - (\chi N)_{sample-ODT}\right]/(\chi N)_{blk-ODT} \approx 0.24 \qquad 1.$$

where $(\chi N)_{bulk-ODT} \approx 10.5$ and $(\chi N)_{sample-ODT} \approx 7.94$. A sample of N = 245 exhibits some degree of order for thicknesses of up to 3L, whereas droplets form on the surfaces of films of thickness h = 4L. The extent to which order would be induced throughout a thick sample would depend on the distance to the substrate and on the proximity of the χN of the sample to the bulk condition $(\chi N)_{bulk-ODT} \approx 10.5$. These results demonstrate that small differences in χN lead to large shifts of the ODT in temperature.

It is important to examine the average chain length dependence of the interlamellar spacings, L, in this system since it can be indicative of the extent of the degree of segregation. Numerous line scans were taken of the brush layer and of the terraces of samples of h < 2L. All measurements were averaged and the data plotted in Figure 2.4. The measurements of the brush layer thickness are represented by circles and those of the terraces represented by triangles. The line drawn through the data, though limited in range, has a slope of 2/3. The 2/3 power law is consistent with strong segregation behavior. Regardless of the slope, the main point is that samples of N > 216 were ordered throughout, for all these films of thickness h < 2L.

The increase of the ODT of the PS-b-PMMA (vacuum) thin films supported by SiO_x/Si substrates relative to the bulk is readily understood. PMMA exhibits a strong affinity with the oxide layer (*H*-bonding), which has the effect of excluding PS from the substrate. PS has a lower surface energy and is preferentially attracted to the free surface, though the free surface interaction is weak in comparison. The action of these two "surface fields" leads to a larger effective interaction parameter between PS and PMMA in the vicinity of the substrate, $\chi_{surf}(PS-PMMA) > \chi_{bulk}(PS-PMMA)$ and an associated higher ODT. The disparity between the two interaction parameters, of course, is diminished at locations away from the substrate.

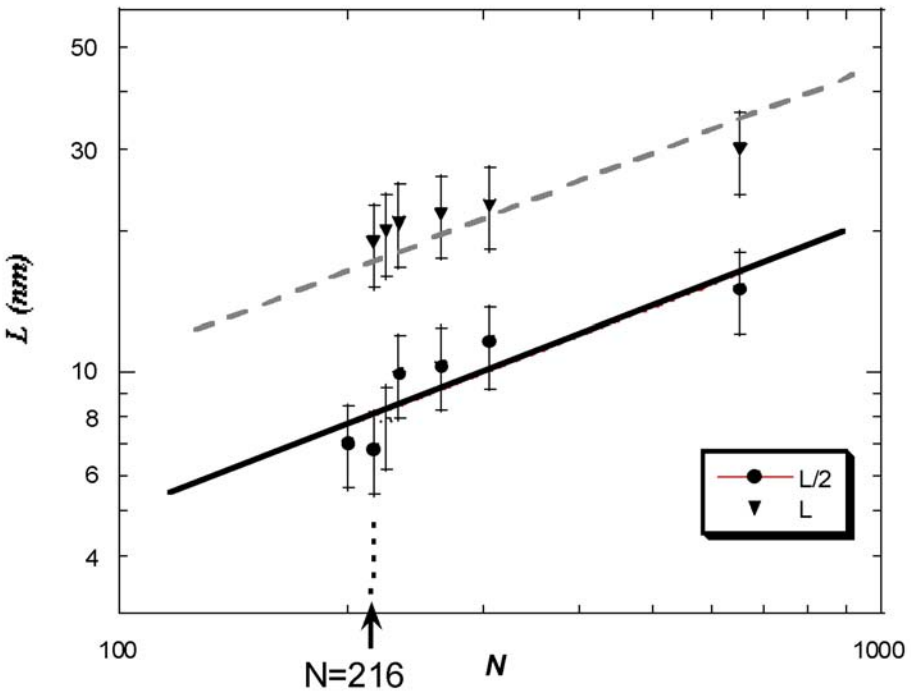

Figure 2.4 The chain length dependencies of interlamellar spacing obtained from the height of the topographical features (L) and from the height of the brush layer (L/2) are shown here. The line drawn through the data has a slope of 2/3.

2.3.2 Diblock copolymer in CO_2 at 170°C

The effect of CO_2 on the ordering transition of the copolymers is now discussed. As mentioned above, bulk studies of PS-b-PMMA indicate that CO_2 should have the effect of enhancing the miscibility, i.e.: lowering the ODT. We found that all thin film samples of $h < 2L$ processed in CO_2 at 170°C and 145 bar exhibited ordering throughout, indicating the opposite behavior. We begin by showing an SFM scan of the sample of N = 201 in Figure 2.5a. The accompanying line scan indicates that a second layer of thickness L, above the brush layer, is ordered (Fig. 2.5b). The surprising observation in Figure 2.5 is that the 20 nm film in CO_2 at 170°C is ordered throughout whereas for the same sample annealed in vacuum at the same temperature the chains above the brush layer are disordered. Recall that, in the bulk, while CO_2 preferentially interacts with the PMMA phase, the relative concentration of CO_2 molecules between the PS and the PMMA phases is reduced due to entropic considerations since the molecules increase their translational entropy by residing in both PS and PMMA phases. Consequently, the relative interactions between the unlike segments are mediated and the effective χ-parameter is lower, leading to a decrease of the ODT.[16] In thin films, supported by a substrate that interacts strongly with one component of the copolymer, on the other hand, the effective $\chi_{PS\text{-}PMMA}$ parameter is larger in the vicinity of the substrate than the bulk. Consequently, in thin film PS-PMMA/CO_2 systems, the ODT is larger than the bulk ODT.

If the same argument used to explain the lowering of the ODT in the bulk is applied here, then the ODT of the thin film PS-PMMA/CO_2 system should be the lower than the ODT of the thin film PS-PMMA/vacuum system. Clearly, it does not work in

this situation. We might begin to understand this observation by considering the following.

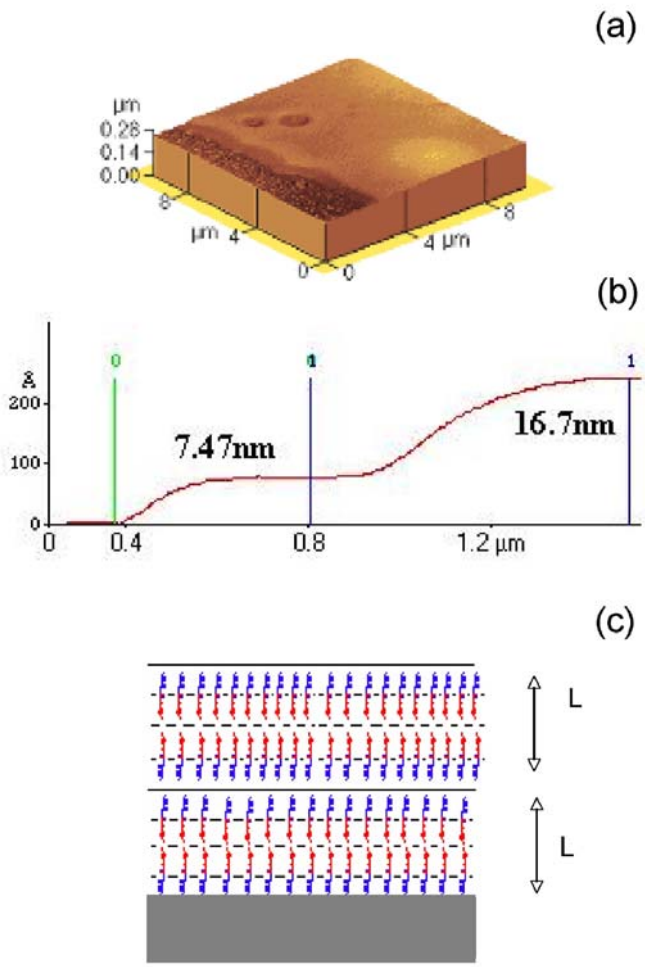

Figure 2.5 Shown here is an SFM scan of the sample of N = 201 and h = 20 nm annealed at 170°C under 145 bar of CO_2. The line scan indicates that unlike the sample in Figure 1, annealed in vacuum at the same temperature, both layers are ordered.

Regardless of the film thickness, the relative interactions between PS and CO_2 and PMMA and CO_2 are different. However, the ordering of the film in CO_2 suggests that the nature of the interactions between CO_2 and each of the polymers is thickness dependent and more importantly, the disparity between the CO_2-PS and CO_2-PMMA interactions in thin films is much larger than in the bulk. There is evidence of such an increasing disparity based on CO_2 devitrification measurements of both polymers.[27, 28] To begin with, in thin films, the T_g of a PMMA film on the SiO_x substrate increases with decreasing film thickness, whereas PS films on the same substrate exhibit the opposite trend. At a temperature of 75°C, for example, a CO_2 pressure of 45 atm is required to plasticize a PS film of 100 nm whereas a pressure of approximately 42 atm is required to plasticize a PMMA film of the same thickness on the same substrate. However, for a PMMA film of 25 nm, a pressure of 15 atm is required whereas for a PS film of the same thickness on the same substrate a pressure of 34 atm, twice as large, is required to plasticize the PS film. In short, the increasing disparity between the interactions of CO_2 between PS and with PMMA with decreasing film thickness would account for the ordering of the film in CO_2. To this end, it should be further emphasized that small changes in enthalpic interactions are associated with large changes in ordering temperatures; the chi parameter has a large entropic, temperature independent, term and a second term that varies as 1/T; large changes in T are associated with small changes in χ.

In a recent publication, Shah et al.[29] perform mean field theoretical calculations to study the stability of diblock copolymer films supported by a neutral substrate as well as of bulk systems, both in the presence of a selective compressible solvent. The authors define a 'layered dewetting temperature' (LDT) at which a periodic double-well minimum appears in the free energy as a function of thickness of a thin diblock copolymer film. This LDT is equivalent to the thin film ODT of our samples. Their

results are in qualitative agreement with our experimental observations, namely, that the LDT lies below the bulk ODT. Further, they investigated the role of the compressibility and selectivity of the solvent. They found that LDT decreases even further as the solvent pressure increases (leading to greater solvent content in the film), but the change is not substantial. For the case of solvent selectivity, they found that greater LDT depressions are obtained if the degree of selectivity increases.

We now briefly discuss two different experimental observations that give us more insight with regards to the degree of segregation imparted by CO_2. A set of samples with degree of polymerization N = 201 was annealed at 110°C, and 145 bar. The sample thickness ranged from 18 nm to 72 nm. Upon inspection of two representative samples under SFM (Fig. 2.6), we see that the films form once again, a brush layer with thickness 1/2L. The morphology of the material sitting on top of the brush is different for the thin film (22nm) compared to the thicker one. Indeed the thin film shows the presence of islands, with height L, as expected (Fig. 2.6a). On the other hand, the thicker sample (33nm) shows a mixed morphology (Fig. 2.6b): It shows the presence of islands (segregated material) on top of a brush. The remaining material shows no evidence of phase segregation, and in fact, a rim indicative of dewetting can be seen. These results highlight the short-range character of the order induced.

To conclude, we discuss the second observation. Figure 2.7 compares the line scans obtained for experiments at 110°C and 60°C. In figure 2.7a, it is clearly seen that the sample annealed at 110°C wets the substrate in an asymmetric fashion. On the other hand, the line scan for the sample 2.7b reveals that the height of the first and second layers is practically the same, indicating that the lamellar structure has gone from asymmetric to symmetric wetting. We propose that this change in wetting behavior is due to a higher CO_2 density at such a low temperature.

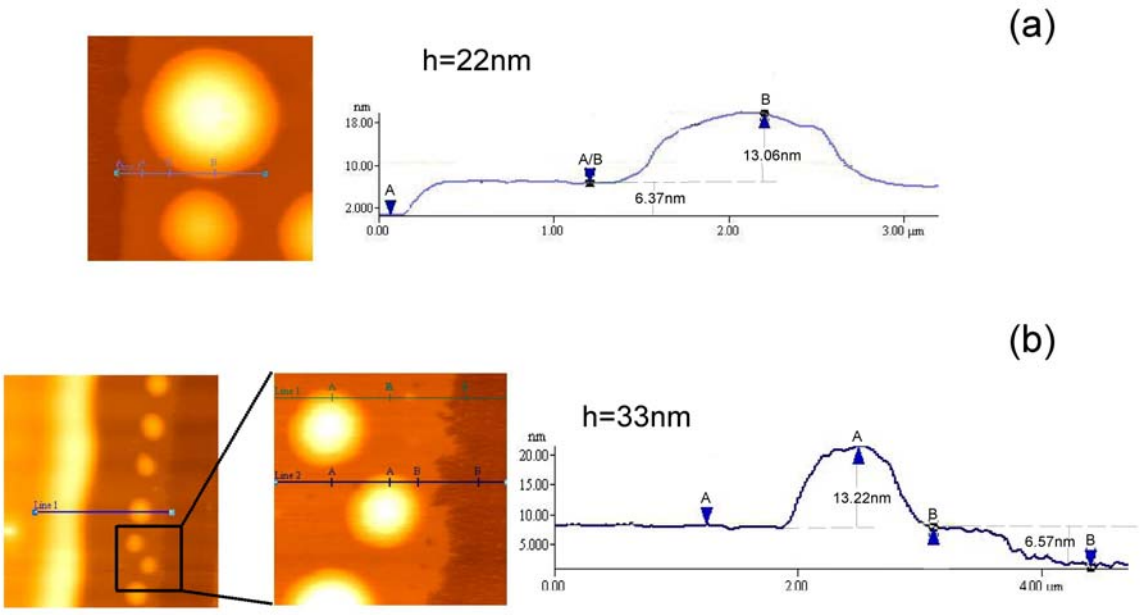

Figure 2.6 Topography images, and line scans of PS-b-PMMA films of degree of polymerization N = 201 annealed at 110°C under 145 bar of supercritical CO_2. (a) Topography and line scans of sample with original thickness h = 22nm. The image is representative of the sample surface: structured islands on top of a segregated brush. (b) Topography and line scans of the same diblock copolymer spin coated to a thickness of h=33nm. The sample has a mixed topography in which structured islands reside on top of a brush layer, but the majority of the material is dewetting, and will eventually form amorphous droplets. This is an indication that enhancement of phase segregation is relatively short-ranged.

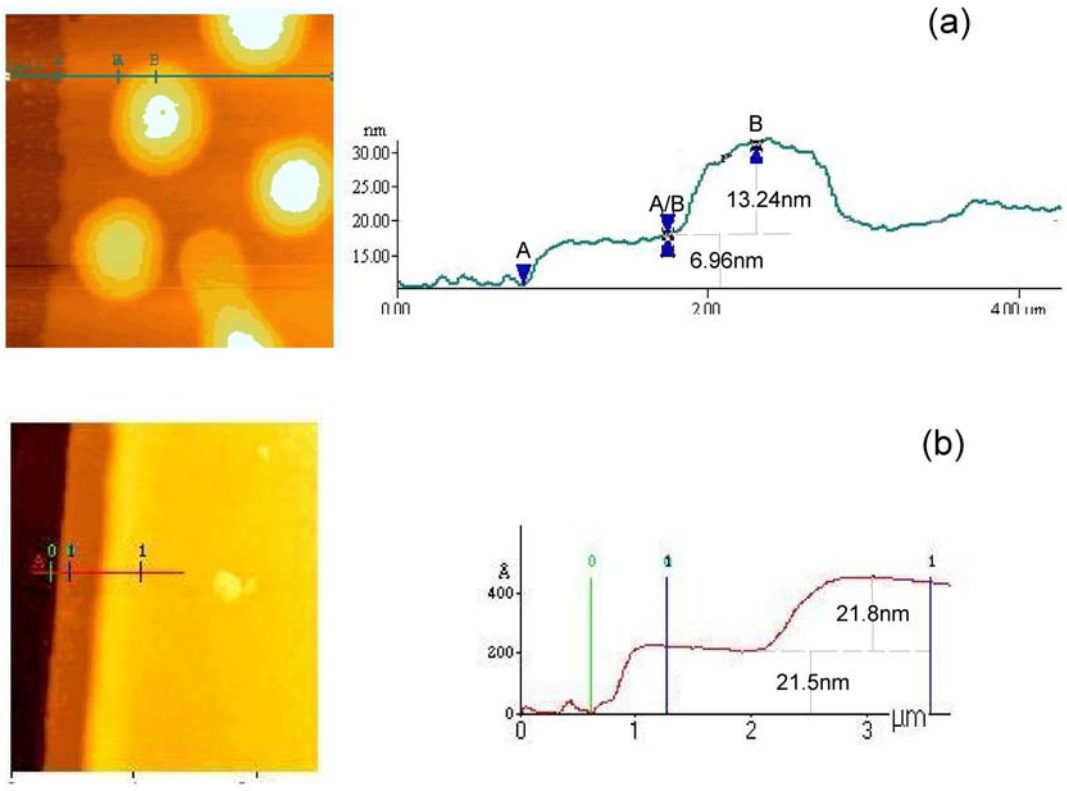

Figure 2.7 Topography images, and line scans of PS-b-PMMA films of degree of polymerization N=201 annealed under 145 bar of supercritical CO_2 at: (a) 110°C, and (b) 60°C. From the images, it can be seen that the system undergoes a shift in wetting behavior from asymmetric at high temperatures to symmetric at low temperatures.

The increase in density has the effect of modifying the interfacial interactions at the free surface: the number of relatively unfavorable interactions between PS and the supercritical fluid increases significantly. A way to minimize its free energy is by allowing PMMA to reside at the free surface, since its interactions with CO_2 are more favorable. This means that the first layer in the film goes from a brush layer to a full lamella. It is important to note this ability to change the wetting characteristics of the diblock copolymer with changes in annealing temperature is likely to be exclusive to supercritical fluids, whose density and solvent quality can be markedly modified with small adjustments of pressure/temperature.

2.4 CONCLUSIONS

Bulk, symmetric, A-b-B diblock copolymers undergo an isotropic-to-lamellar transition below the ODT, characterized by the condition $\chi_{bulk}N > 10.5$. We have shown that thin film PS-b-PMMA copolymers undergo this transition for $\chi_{bulk}N < 10.5$, a substrate induced transition. This is because interactions of PMMA with the substrate leads to a larger effective $\chi_{substrate} > \chi_{bulk}$ in the vicinity of the substrate compared to the bulk.

The significant finding is that experiments conducted in the environment of a compressible fluid, which is generally expected to reduce the ODT (in fact known to induce mixing in the PS-b-PMMA bulk) shows the opposite effect. Our results reveal that the effective ODT of this system is not only larger than the bulk, but also larger than the system in vacuum environments. This result is particularly noteworthy because CO_2 is known to plasticize both PS and PMMA homopolymers and hence decrease their viscosities considerably. However in this case, diblock copolymers of the same polymers self-organize. The implication is that whereas it would be easy to process thin film

homopolymers because of the reduced viscosity, the effective viscosity of the self-organized diblock copolymers would be much larger that one would initially anticipate. Furthermore, we found evidence that suggests that the enhancing effect of CO_2 on the phase segregation of confined diblock copolymers might be limited to less than two lamellar spacings. Additionally, we found that by carefully adjusting the density of supercritical CO_2 a shift in the wetting characteristics of the film can be obtained. The consequences of this are far reaching with regard to processing.

2.5 REFERENCES

1. Anastasiadis, S. H.; Russell, T. P.; Satija, S. K.; Majkrzak, C. F. *Physical Review* Letters 1989, 62, (16), 1852-1855.

2. Bates, F. S.; Fredrickson, G. H. *Annual Review of Physical Chemistry* **1990,** 41, 525-557.

3. Fredrickson, G. H. *Macromolecules* **1987,** 20, (10), 2535-2542.

4. Green, P. F. *Journal of Polymer Science Part B-Polymer Physics* **2003,** 41, (19), 2219-2235.

5. Hamley, I. W., *The physics of block copolymers*. Oxford University Press: Oxford, 1998.

6. Mansky, P.; Tsui, O. K. C.; Russell, T. P.; Gallot, Y. *Macromolecules* **1999,** 32, (15), 4832-4837.

7. Black, C. T.; Guarini, K. W.; Milkove, K. R.; Baker, S. M.; Russell, T. P.; Tuominen, M. T. *Applied Physics Letters* **2001,** 79, (3), 409-411.

8. Chou, S. Y.; Wei, M. S.; Krauss, P. R.; Fischer, P. B. *Journal of Applied Physics* **1994,** 76, (10), 6673-6675.

9. De Rosa, C.; Park, C.; Thomas, E. L.; Lotz, B. *Nature* **2000,** 405, (6785), 433-437.

10. Guarini, K. W.; Black, C. T.; Milkove, K. R.; Sandstrom, R. L. *Journal of Vacuum Science & Technology B* **2001,** 19, (6), 2784-2788.

11. Pai, R. A.; Humayun, R.; Schulberg, M. T.; Sengupta, A.; Sun, J. N.; Watkins, J. J. *Science* **2004,** 303, (5657), 507-510.

12. Park, M.; Harrison, C.; Chaikin, P. M.; Register, R. A.; Adamson, D. H. *Science* **1997,** 276, (5317), 1401-1404.

13. Zhang, Y.; Gangwani, K. K.; Lemert, R. M. *Journal of Supercritical Fluids* **1997,** 11, (1-2), 115-134.

14. RamachandraRao, V. S.; Gupta, R. R.; Russell, T. P.; Watkins, J. J. *Macromolecules* **2001,** 34, (23), 7923-7925.

15. RamachandraRao, V. S.; Watkins, J. J. *Macromolecules* **2000,** 33, (14), 5143-5152.

16. Vogt, B. D.; Brown, G. D.; RamachandraRao, V. S.; Watkins, J. J. *Macromolecules* **1999,** 32, (23), 7907-7912.

17. Vogt, B. D.; RamachandraRao, V. S.; Gupta, R. R.; Lavery, K. A.; Francis, T. J.; Russell, T. P.; Watkins, J. J. *Macromolecules* **2003,** 36, (11), 4029-4036.

18. Watkins, J. J.; Brown, G. D.; RamachandraRao, V. S.; Pollard, M. A.; Russell, T. P. *Macromolecules* **1999,** 32, (23), 7737-7740.

19. Stafford, C. M.; Russell, T. P.; McCarthy, T. J. *Macromolecules* **1999,** 32, (22), 7610-7616.

20. Smith, M. D.; Green, P. F.; Saunders, R. *Macromolecules* **1999,** 32, (25), 8392-8398.

21. Shull, K. R. *Macromolecules* **1992,** 25, (8), 2122-2133.

22. Orso, K. A.; Green, P. F. *Macromolecules* **1999,** 32, (4), 1087-1092.

23. Menelle, A.; Russell, T. P.; Anastasiadis, S. H.; Satija, S. K.; Majkrzak, C. F. *Physical Review Letters* **1992,** 68, (1), 67-70.

24. Limary, R.; Green, P. F.; Shull, K. R. *European Physical Journal E* **2002,** 8, (2), 103-110.

25. Limary, R.; Green, P. F. *Macromolecules* **2002,** 35, (17), 6486-6489.

26. Limary, R.; Green, P. F. *Langmuir* **1999,** 15, (17), 5617-5622.

27. Pham, J. Q.; Sirard, S. M.; Johnston, K. P.; Green, P. F. *Physical Review Letters* **2003,** 91, (17), -.

28. Pham, J. Q.; Johnston, K. P.; Green, P. F. *Journal of Physical Chemistry B* **2004,** 108, (11), 3457-3461.

29. Shah, M.; Pryamitsyn, V.; Ganesan, V. *Journal of Physical Chemistry B* **2007,** 111, (2), 402-407.

Chapter 3: Nanoparticle-Induced Shift in the Order Disorder Transition of Confined Diblock Copolymers

3.1 INTRODUCTION

During the last few decades, organic and inorganic fillers have been added to polymers with the goal of improving their mechanical properties for different applications. Fillers such as carbon black, talc and fiber glass were added to different polymers to fabricate macroscopic composites. The mechanisms by which the mechanical properties of these materials are improved are well understood. In recent years, it has been shown that more significant enhancements of physical properties can be achieved with the use of fillers with nanoscopic dimensions, comparable to the average dimensions of a polymer chain or smaller. Organo clays, fullerenes (carbon nanotubes and their derivatives, C_{60} etc.), metallic nanoparticles and semiconducting nanoparticles (quantum dots) represent examples of nanoparticles that can be incorporated into polymer hosts to create polymer nocomposites PNCs).

Depending on the polymer and the properties of the nanoparticles, many properties of the system are changed[1-10]: chain relaxation times, diffusion, viscosity, morphology, wetting, mechanical, thermal, electrical and optical properties. The properties exhibited by PNCs, are more significant, and often counterintuitive, in comparison to conventional macroscopic composites. The property enhancements exceed predictions based on conventional theories used to describe the behavior of macroscopic composites. This new class of materials has the potential to enable some

exciting new technologies in the fields of photonics, sensing, and catalysis, to name just a few.

The properties of PNCs are extremely sensitive to the spatial distribution and ordering of the nanoparticles throughout polymer host. Control of the dispersion is difficult because the particles exhibit a strong tendency to aggregate.[11, 12] One strategy that has gained much attention recently is to incorporate the particles into an A-b-B diblock copolymer host, thereby taking advantage of the compatibility between the particle and one of the components. The use of A-b-B diblock copolymers as the polymeric matrix is of particular interest due to their rich phase behavior that allows them to self-assemble into three-dimensional periodic nanostructures, as mentioned in Chapter 1.

Generally, when nanoparticles are added to such phase segregated geometrical structures, the particles segregate to the regions of the sample with which they are thermodynamically most compatible.[13-17] For example, if the A-phases form spheres, then the nanoparticles that are compatible with the A component will form a discontinuous phase because they, in principle, will reside in the A phase only. Depending on the relative size of the particles in relation to the dimensions of a domain (D/L), the strength of the relative interactions of the particles with the phases (χ), the volume fraction of the particles, and the particle-particle interactions, a wide range of morphologies are possible.[2, 13, 18-20]

There have been a number of challenges associated with the incorporation of nanoparticles within copolymer phases. Particle-particle interactions are especially problematic in practice, since such interactions can have a dominant effect on the free energy. One strategy that is often used is to graft polymer chains of different lengths at varying densities onto the particles. By doing this, control over the interactions with the

polymer host may be exercised. We will address this issue later in this paper as it forms the basis for the experiments discussed here.

Most of the attention thus far has concentrated on bulk systems, and very little on thin films. In this study, we are interested in understanding the effect of polystyrene (PS)-capped gold nanoparticles on the morphology of low molecular weight thin films of symmetric poly(styrene-b-methyl methacrylate) (PS-b-PMMA) diblock copolymers. The films were supported on silicon nitride (Si_3N_4), which is selective towards the PMMA block, and their thickness (h) ranged from $1/2L < h < 2L$, where L is the lamellar domain size. The total diameter of the particles and grafted brush layers, D, is comparable to or smaller than L of the copolymer chains. We show that the nanoparticles induce lamellar order to the system, even beyond what is expected for highly confined diblock films.

3.2 EXPERIMENTAL

3.2.1Nanoparticle synthesis and characterization

Gold nanocrystals were synthesized using a modified version of the two-phase arrested precipitation method first reported by Brust et al.[21, 22] Two separate reaction batches were prepared; the first one was stopped at an early time to obtain nanoparticles with an average diameter of 1.8 nm. The second batch was allowed to react until the average nanoparticle core size reached an average value of 5 nm. The surface of both types of nanoparticles was passivated with thiol-terminated polystyrene chains with molecular weight of 1000g/mol (degree of polymerization, N = 10). The average size of the gold cores was measured from scanning transmission electron microscope (STEM) images of the nanoparticles, which were evaporated from dilute solution onto a regular copper TEM grid (Ted Pella, Inc.). STEM was performed on a JEOL 2010 microscope

operated at an accelerating voltage of 200 kV in scanning mode using a high-angle annular dark-field detector. Gold core diameter measurements were taken from over 300 particles using Image J software. Measurements of the inter-particle separation distances allowed us to estimate the thickness of the grafted brush (~ 2nm).

3.2.2 Sample preparation

Symmetric diblock copolymers of polystyrene and poly(methylmethacrylate), (PS-b-PMMA) of number average molecular weights M_n = 20,500 g/mol and M_n = 65,500 g/mol were purchased from Polysciences, Inc. and used as received. Toluene solutions of each diblock copolymer were blended in order to obtain mixtures with average degrees of polymerization ranging from 201 to 306. These solutions were then mixed with solutions of each nanoparticle size, at two different concentrations, 0.1 and 1% by weight of gold.

The nanocomposite solutions were spin coated onto silicon wafers with a 100 nm silicon nitride layer grown by LPCVD (WaferNet, Inc.). The resulting film thicknesses ranged from 22 to 28 nm. A second set of neat diblock films was prepared as a control experiment.

After spin coating, the nanocomposite samples were annealed at 170°C under a vacuum for 16 h, which is sufficient for the morphology of the films to develop. The topography of these films was observed using scanning probe microscopy to assess the formation of phase segregated structures and their swelling.

3.3 RESULTS AND DISCUSSION

3.3.1 Shifts of the Order-Disorder Transition in Diblock Copolymer/Nanoparticle Films

Our findings regarding the effect of adding selective nanoparticles to PS-b-PMMA thin films are summarized in Figures 3.1-3.3. Let us first discuss the phase behavior of the pure diblock films (Figs. 3.11a to 3.1c). At the experimental conditions used, the corresponding χN values of these films are 7.4, 7.6, and 7.9, respectively. All the samples show the presence of a phase segregated brush layer, with a height corresponding to half the lamellar spacing. The phase segregation of this layer is driven by the presence of the substrate which is selective towards one of the blocks (in this case PMMA)[23-25]. Upon inspection of images 3.1a and 3.1b, one can see droplets on top of the brush layer; these droplets are made of phase mixed material, since they are not commensurate with the underlying brush. A schematic representation of the configuration of the chains in the films above their T_{ODT} is shown in figure 3.4a. On the other hand, the sample shown in figure 3.1c clearly shows the formation of a second layer on top of the brush. This second layer is of height ~ L, which means that all the material in the film has undergone microphase segregation and formed lamellar structures (Fig. 3.4b). Therefore, we consider that the location of an order-disorder transition lies between the values of $7.6 < \chi N < 7.9$. These values are consistent with previous experimental results of PS-b-PMMA thin films spin coated on Si/SiOx substrates.[26]

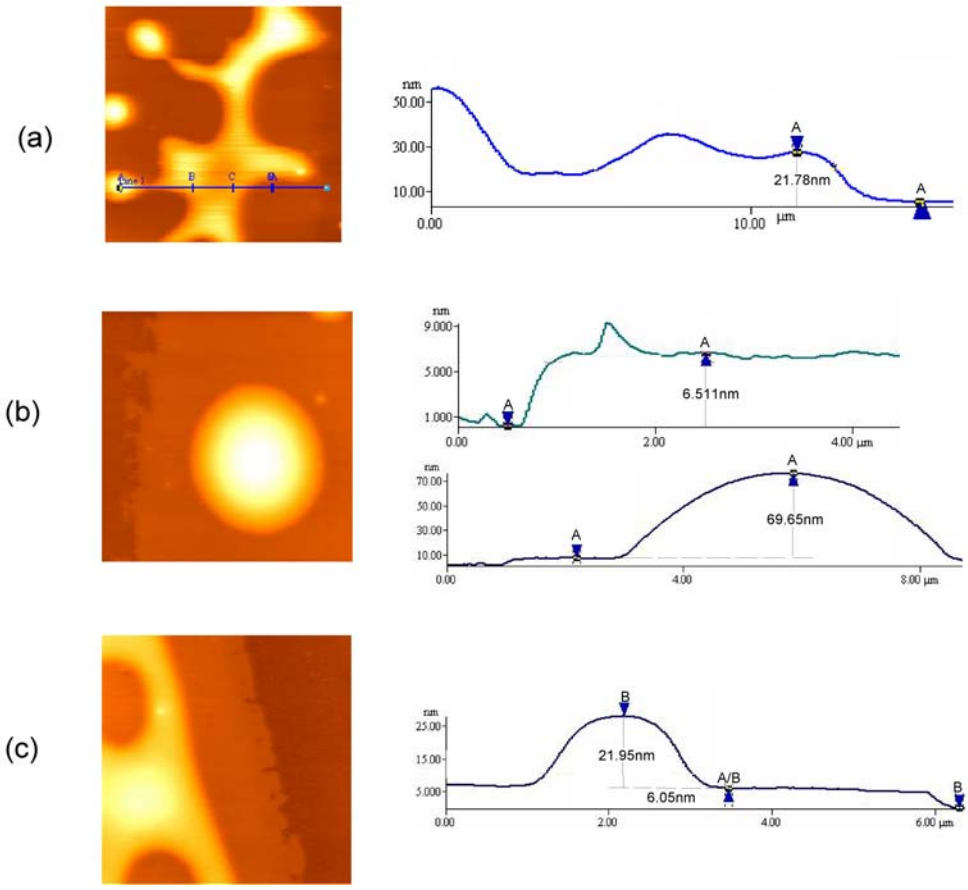

Figure 3.1 Topographic SFM images and corresponding line scans of neat PS-b-PMMA films after annealing for 16 h at 170°C. The degree of polymerization of each sample is (a) 201, (b) 208, and (c) 216.

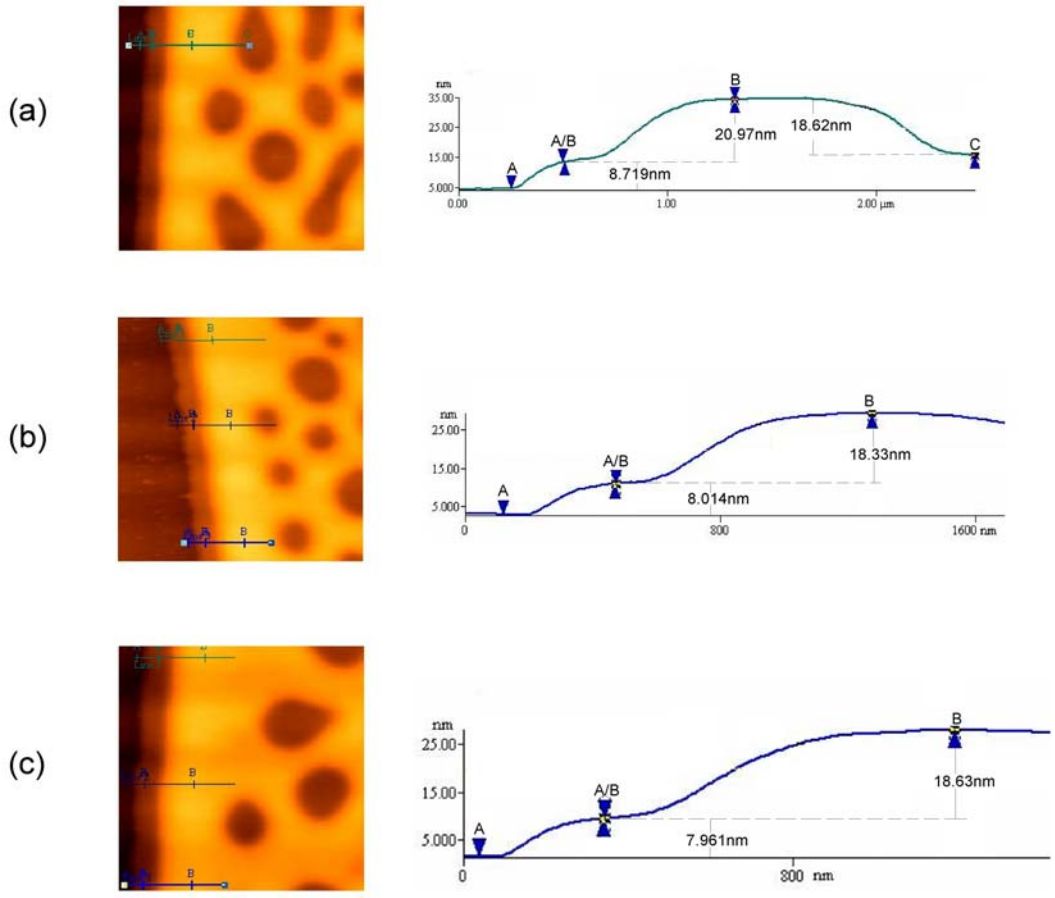

Figure 3.2 Topographic SFM images and corresponding line scans of nanocomposite films of 1% wt. gold nanoparticle (d = 2nm)/PS-b-PMMA after annealing for 16 h at 170°C. The degree of polymerization of each sample is (a) 201, (b) 208, and (c) 216.

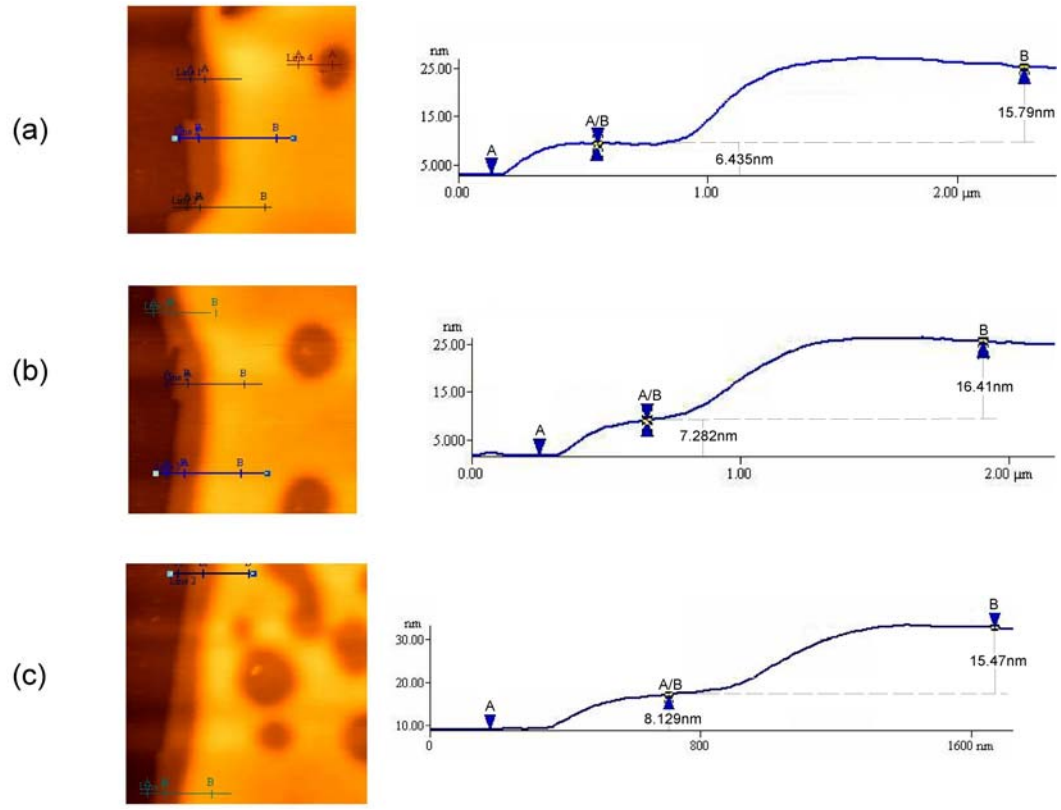

Figure 3.3 Topographic SFM images and corresponding line scans of nanocomposite films of 1% wt. gold nanoparticle (d = 5nm)/PS-b-PMMA after annealing for 16 h at 170°C. The degree of polymerization of each sample is (a) 201, (b) 208, and (c) 216.

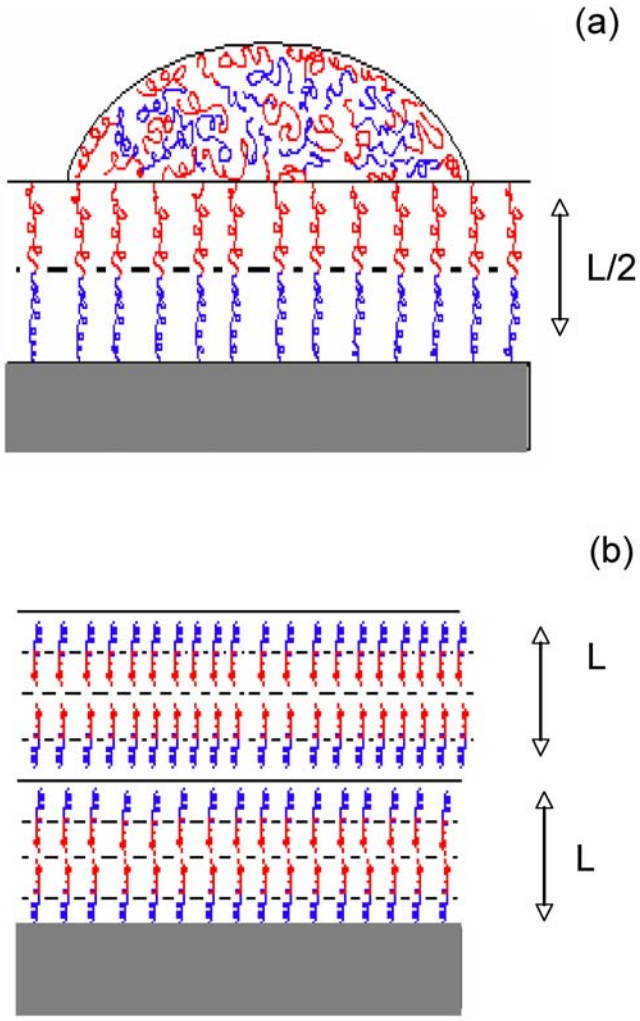

Figure 3.4 Schematic of the different conformation of a block copolymer melt (a) in a disordered state, and (b) in an ordered state.

We now turn our attention to the nanocomposite films. Figures 3.2a to 3.2c show the topography of PS-b-PMMA diblock films filled with PS-covered gold nanoparticles with d = 2nm. The SFM images show that the samples formed a bilayer structure after the annealing process. The second layer of the samples presents holes of uniform height throughout the surface. This kind of topography is commonly observed in lamellar structures of diblock copolymer films when there is not enough material to complete a full lamella. This finding suggests that phase segregation may have been induced by the presence of nanoparticles. Indeed, upon measuring the height at various points throughout the sample, we find that the average value lies very close to that of the lamellar period. One further observation that leads us to believe that phase segregation has occurred is the fact that the holes lack the presence of rims. This is an indication that the holes are not growing; therefore the material on top of the brush layer was not evolving into amorphous droplets. The previous description is also applicable to the samples prepared with the PS coated nanoparticles with core diameter of 5 nm (Figures 3.3a to 3.3c). We therefore conclude that both types of nanoparticles have induced a shift of the ordering transition in the films.

As mentioned earlier, several theoretical and experimental studies have addressed the influence of nanoparticles on the phase behavior of diblock copolymers. However, only a small number have focused on the order-disorder transition temperature. For example, Chervanyov and Balazs[27] have shown that the addition of non-selective nanoparticles to an ordered copolymer can increase the magnitude of the critical value of $(\chi N)_{ODT}$, smaller values of D/L having a larger effect. Moreover, the magnitude increases with increasing nanoparticle concentration. More generally, theoretical calculations and simulations show that phase mixing is promoted when nonselective nanoparticles are added to the block copolymer blend.[18, 19] This occurs via a dilution

effect, whereby the nanocomposite lowers its free energy by localizing the nanofillers at the A-B interface, where they can screen unfavorable contacts between dissimilar monomers. This leads to a broadening of the A-B interface, and eventually gives rise to a disordered morphology.

Theoretical calculations by Huh et al.[20] show a marked reduction of the order-disorder temperature when selective nanoparticles are added. This effect is more pronounced when the particles are small compared to the radius of gyration of the selective block.

Experimental observation of nanoparticle-induced phase mixing was reported by Hamdoun[15], wherein relatively high loadings ($\phi \sim 0.25$) of Fe_2O_3 nanoparticles are seen to destroy the lamellar ordering of a PS-b-PMMA film (M_n = 92,000) of undetermined thickness. Further, Jain et al.[28] observed that low loadings of selective silica nanofillers of different dimensionalities induced a drop in the order-disorder temperature of symmetric PS-b-PI copolymer. The authors suggest that the nanofillers provide nucleation sites for the melting process, where density fluctuations are larger.

It is clear now that the results presented in this work have not been predicted theoretically, and that to the best of our knowledge, have not been observed experimentally either. However, we can make use of the results obtained by Reister and Fredrickson[29] to understand our experimental observations. In their work, it is shown that a single particle having favorable interactions with one of the blocks in a disordered diblock copolymer melt can actually induce phase segregation in the vicinity of its surface. Even though the polymer chains are above their T_{ODT}, a lamellar structure with thickness equal to the amplitude of the oscillatory density profile. This profile decreases with increasing distance from the particle. Upon addition of a second particle to the disordered melt, the interaction between particles creates 'density waves' which can

interfere either constructively or destructively depending on the separation distance. It is important to emphasize here that even though the monomer-particle interaction is short-ranged, the resulting density profile is long ranged, on the order of several radii of gyration.

Interestingly, we can also gain some insight to the nanoparticle-induced phase segregation in our films by looking at earlier theoretical and experimental results on the phase behavior of A-b-B diblock copolymer/A homopolymer blends.[30, 31] When chains of homopolymer A are added to a symmetric diblock, they will reside preferentially within the domains of the A block to avoid unfavorable enthalpic interactions with the B monomers. However, the distribution of the homopolymer within the A block will depend on its molecular weight. In the limit of very low molecular weight, the homopolymer acts as a solvent molecule, and reside preferentially at the A/B interface, thereby diluting the number of unfavorable interactions and lowering the interfacial tension. This leads to a reduction of the order-disorder transition temperature, T_{ODT}, because the effective interaction parameter is reduced. When the molecular weight of the homopolymer is low, it will tend to distribute uniformly across the domain, to increase the translational entropy. As the molecular weight of the homopolymer is increased, the chains tend to be localized at the center of the domains, to avoid the entropic cost of stretching by the copolymer chains in the A block. This has been observed to result in an increase of the T_{ODT}. Since in our experiments, the nanoparticle size is comparable to the lamellar domain (considering core diameter and shell thickness), we think that a similar effect is increasing the T_{ODT} of our films. In a recent publication by Bockstaller et al.,[17] the location of nanoparticles within a selective domain was studied as a function of the ratio d/L, where d is the particle diameter and L is the lamellar spacing of the diblock copolymer. They observed that nanoparticles segregated preferentially to the A/B

interfaces in systems with $d/L \leq 0.2$; otherwise, the nanoparticles are mainly located at the center of the appropriate domains. In our experiments, both our nanoparticles are in the latter regime, considering their effective size, so we would expect them to be localized towards the center of the PS domain.

Finally, it is important to remember that our diblock nanocomposite films are highly confined, on the order of 3/2L, and that under these conditions, the presence of interfaces has been shown to induce significant phase segregation. We conclude that our results can be understood by considering all these contributions acting simultaneously on the nanocomposite films.

3.3.2 Lamellar Domain Swelling

We now discuss the size of the lamellar domains throughout the samples. Figure 3.5 compares the measured average values of each layer for the neat diblock copolymer samples to that for the nanocomposites prepared with the small nanoparticles. As can be seen from the plot, the lamellar domain spacing measured for the nanocomposite films with 0.1% Au is in general comparable to the neat diblock copolymer values. This is not surprising since there is a very low content of nanofiller. On the other hand, the values measured for the nanocomposite films with 1%Au content seem to fall below the value measured for the neat films. This is in contrast to what is expected for selective nanoparticles. For instance, Schultz et al.[18] observed that the total lamellar spacing increases upon addition of selective nanoparticles. This type of behavior can be understood as that of swelling by a selective solvent or homopolymer chain. It is interesting to note that the degree of swelling by the selective block is expected to decrease with increasing nanoparticle size. The reason for this is because a large nanoparticle imposes a greater penalty in conformational entropy of the block, and

therefore is segregated to the center of the domain to allow the chains to relax, and therefore become less stretched. On the other hand, the only instance in which lamellar domain size is expected to decrease is when non-selective nanoparticles are added.[19] The reduction in lamellar domain dimensions stems from the fact that non-selective nanoparticles allocate themselves at the A/B boundary, effectively reducing the number of unfavorable contacts between dissimilar monomers. This 'dilution' effect allows the diblock chains to decrease their degree of stretching. We believe that further experiments should be carried out with larger concentration of nanoparticles to be able to properly evaluate this unexpected result.

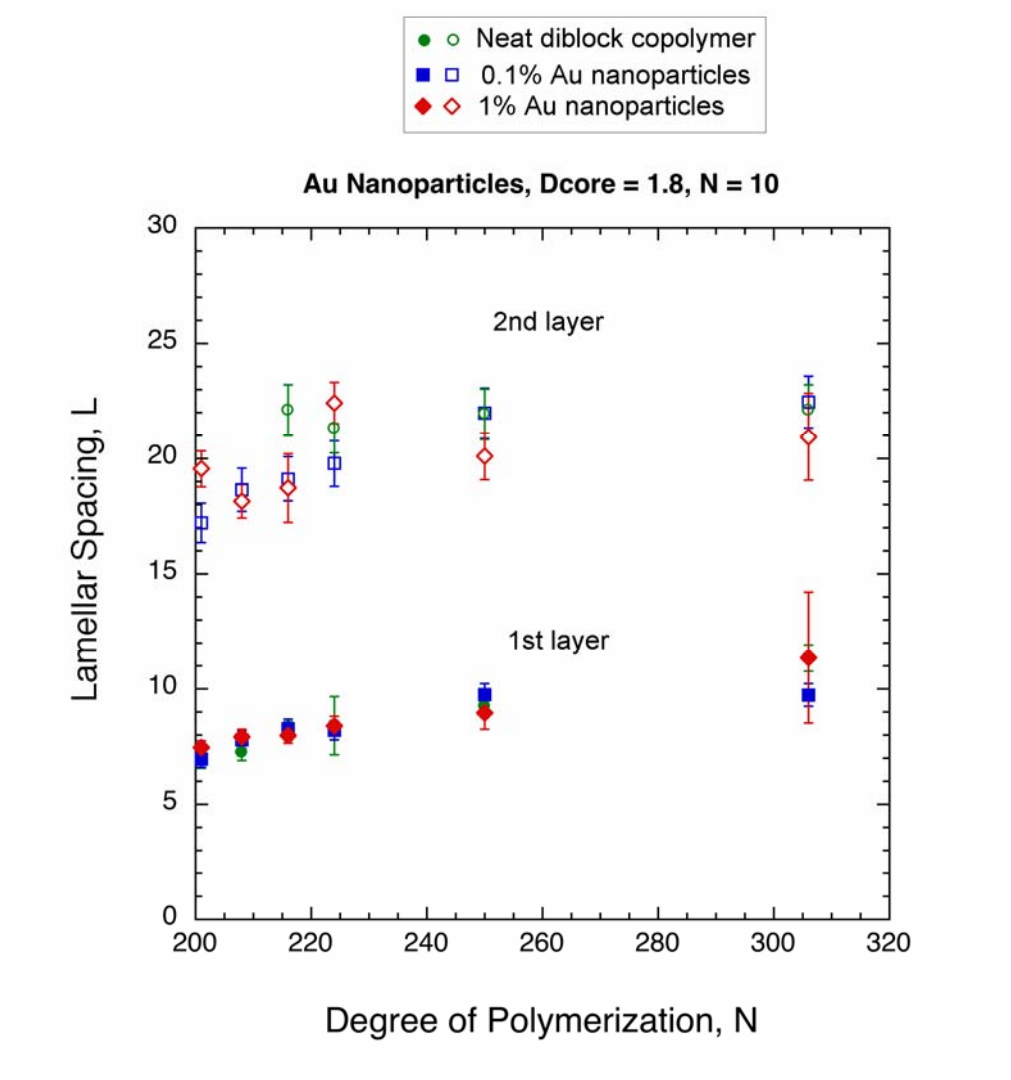

Figure 3.5 Measurements of lamellar structures in PS-b-PMMA films after annealing at 170°C for 16 h.

3.4 CONCLUSIONS

In this work, we have studied the effects of adding selective nanoparticles to a confined symmetric PS-b-PMMA diblock copolymer on its ordering transition temperature and on the size of its lamellar spacing. We first determined the order disorder transition for the neat system, to evaluate the effect of confinement and substrate/polymer interactions. As expected, the ordering temperature was higher than that for a bulk diblock copolymer with the same average degree of polymerization, N. The ordering transition occurs at $7.6 < \chi N < 7.9$. Addition of PS-coated nanoparticles resulted in the formation of lamellar structures in all of our samples, indicating that selective nanoparticles can induce phase segregation. This is an unexpected result, since most theoretical calculations for selective nanoparticles show that lamellar structure is lost at high nanoparticle loadings (volume fraction, $\phi > 0.1$). In summary, we propose that the results reported in this work are a consequence of three factors: a) Enrichment of PS monomers near the nanoparticle surface, resulting in segregation of the diblock chains, as explained by Reister and Fredrickson. b) The size of the nanoparticles is comparable to the domain spacing of the diblock copolymer chains, leading to a situation similar to the case where adding small amounts of large homopolymer into a symmetric diblock decreases its ODT. c) High degree of confinement. As has been seen in previous work, the presence of interfaces has the effect of increasing the repulsive interactions between the blocks forming the copolymer, leading to an effective interaction parameter $\chi_{eff} > \chi_{A\text{-}B}$

3.5 REFERENCES

1. Bliznyuk, V.; Ruhstaller, B.; Brock, P. J.; Scherf, U.; Carter, S. A. *Advanced Materials* **1999,** 11, (15), 1257-+.

2. Buxton, G. A.; Lee, J. Y.; Balazs, A. C. *Macromolecules* **2003,** 36, (25), 9631-9637.

3. Krishnamoorti, R.; Yurekli, K. *Current Opinion in Colloid & Interface Science* **2001,** 6, (5-6), 464-470.

4. Krishnan, R. S.; Mackay, M. E.; Hawker, C. J.; Van Horn, B. *Langmuir* **2005,** 21, (13), 5770-5776.

5. Li, C. X.; Wu, J. T.; Zhao, J.; Zhao, D. L.; Fan, Q. R. *European Polymer Journal* **2004,** 40, (8), 1807-1814.

6. Mackay, M. E.; Dao, T. T.; Tuteja, A.; Ho, D. L.; Van Horn, B.; Kim, H. C.; Hawker, C. J. *Nature Materials* **2003,** 2, (11), 762-766.

7. Papakonstantopoulos, G. J.; Yoshimoto, K.; Doxastakis, M.; Nealey, P. F.; de Pablo, J. J. *Physical Review E* **2005,** 72, (3), -.

8. Potschke, P.; Dudkin, S. M.; Alig, I. *Polymer* **2003,** 44, (17), 5023-5030.

9. Starr, F. W.; Schroder, T. B.; Glotzer, S. C. *Physical Review E* **2001,** 6402, (2), -.

10. Sternstein, S. S.; Zhu, A. J. *Macromolecules* **2002,** 35, (19), 7262-7273.

11. Huang, F.; Zhang, H. Z.; Banfield, J. F. *Journal of Physical Chemistry B* **2003,** 107, (38), 10470-10475.

12. Zhang, H. Z.; Banfield, J. F. *Nano Letters* **2004,** 4, (4), 713-718.

13. Thompson, R. B.; Ginzburg, V. V.; Matsen, M. W.; Balazs, A. C. *Science* **2001,** 292, (5526), 2469-2472.

14. Schmaltz, B.; Brinkmann, M.; Mathis, C. *Macromolecules* **2004,** 37, 9056-9063.

15. Hamdoun, B. *European Polymer Journal* **2004,** 40, (7), 1559-1564.

16. Chiu, J. J.; Kim, B. J.; Kramer, E. J.; Pine, D. J. *Journal of the American Chemical Society* **2005,** 127, (14), 5036-5037.

17. Bockstaller, M. R.; Mickiewicz, R. A.; Thomas, E. L. *Advanced Materials* **2005,** 17, (11), 1331-1349.

18. Schultz, A. J.; Hall, C. K.; Genzer, J. *Macromolecules* **2005,** 38, (7), 3007-3016.

19. Pryamitsyn, V.; Ganesan, V. *Macromolecules* **2006,** 39, (24), 8499-8510.

20. Huh, J.; Ginzburg, V. V.; Balazs, A. C. *Macromolecules* **2000,** 33, (21), 8085-8096.

21. Brust, M.; Walker, M.; Bethell, D.; Schiffrin, D. J.; Whyman, R. *Journal of the Chemical Society. Chemical Communications* **1994**, 801.

22. Brust, M.; Fink, J.; Bethell, D.; Schiffrin, D. J.; Kiely, C. *Journal of the American Chemical Society* **1995,** Communications, 1655.

23. Limary, R.; Green, P. F.; Shull, K. R. *European Physical Journal E* **2002,** 8, (2), 103-110.

24. Anastasiadis, S. H.; Russell, T. P.; Satija, S. K.; Majkrzak, C. F. *Physical Review Letters* **1989,** 62, (16), 1852-1855.

25. Mansky, P.; Tsui, O. K. C.; Russell, T. P.; Gallot, Y. *Macromolecules* **1999,** 32, (15), 4832-4837.

26. Arceo, A.; Green, P. F. *Journal of Physical Chemistry B* **2005,** 109, (15), 6958-6962.

27. Chervanyov, A. I.; Balazs, A. C. *Journal of Chemical Physics* **2003,** 119, (6), 3529-3534.

28. Jain, A.; Gutmann, J. S.; Garcia, C. B. W.; Zhang, Y. M.; Tate, M. W.; Gruner, S. M.; Wiesner, U. *Macromolecules* **2002,** 35, (13), 4862-4865.

29. Reister, E.; Fredrickson, G. H. *Macromolecules* **2004,** 37, (12), 4718-4730.

30. Likhtman, A. E.; Semenov, A. N. *Macromolecules* **1997,** 30, (23), 7273-7278.

31. Matsen, M. W. *Macromolecules* **1995,** 28, (17), 5765-5773.

Chapter 4: Influence of Entropic Constraints on the Glass Transition of Nanocomposite Films

4.1 INTRODUCTION

The addition of nanoscopic fillers to produce new composite materials has gained widespread interest in recent years, due to the remarkable property enhancements that can be achieved at low loadings. Further, novel nanofillers differ from traditional ones in that they exhibit a wide range of size dependent optical, electrical and mechanical properties that can be exploited to obtain sophisticated functional composites. The unique behavior of polymer nanocomposites is attributed to their large surface area to volume ratio, which maximizes contact between filler and matrix. It is therefore important to obtain a great degree of dispersion of the fillers into the matrix; however, it is often found that this is difficult to achieve. A common approach to circumvent this issue is by chemically modifying the surface of the filler by grafting polymer chains to compatibilize it with the surrounding matrix.

Recently, it has been observed that the glass transition of polymer nanocomposites differs from that of the neat polymer depending on the strength and type of polymer-filler interactions.[1-7] Until now, changes on the glass transition of polymer nanocomposites have been observed to follow a simple rule, based on the nature of enthalpic interactions between filler surface and monomer units in the chain: ΔT_g increases if filler-monomer interactions are favorable and the opposite occurs for unfavorable interactions. The underlying reason for this behavior is the monomer density in the vicinity of the nanofiller surface, namely, monomers that have strong favorable interactions with the surface are more tightly packed in comparison to the monomers in

the bulk of the matrix.[8-12] This increase in monomer density restricts the configurational freedom of the chains surrounding the filler, therefore slowing down the overall dynamics of the system.[9-11, 13]

Because in polymer nanocomposites there is a large volume of polymer affected by the presence of interfaces, their glass transition behavior is often compared to that of polymer thin films supported by a solid substrate,[3, 11] of which we have given a brief overview in Chapter 1. It suffices to remind the reader that the T_g of polymers that have specific interactions with a substrate is seen to increase with decreasing film thickness, whereas polymers that lack such interactions actually decrease their T_g upon a decrease in thickness. Several models have been proposed to understand this behavior.[14-19] One of the models most successful at describing the wide variety of aspects observed in the thickness dependence of T_g is based on dynamic heterogeneity within the film, proposed by Long and Lequeux.[15] Generally, they hypothesize that within a film there is a coexistence of fast and slow domains, the relative amounts of which depend on the proximity to T_g, when percolation is supposed to occur throughout the film. Once percolation occurs, the slow domains dominate the overall dynamics of the confined polymer.

As stated earlier, most experimental observations of the behavior of the glass transition of polymer nanocomposites have been understood in view of the predominant enthalpic interactions in the system for hard-sphere nanoparticle/polymer mixtures. Hence little is understood of the impact of the different entropic interactions that can arise in athermal mixtures with polymer-coated nanofillers, such as entropy of mixing of the filler, conformational entropy of the chains, and brush-matrix entropic interactions. In the present work we address this issue by using a model system in which the aforementioned entropic driving forces are controlled by varying the molecular size of

ligands and polymer matrix, as well as nanoparticle core size. Our results show that even in the absence of enthalpic interactions, the glass transition of polymer nanocomposites can be affected by the balance of entropic forces.

4.2 EXPERIMENTAL SECTION

4.2.1 Nanoparticle synthesis and characterization

Gold nanocrystals were synthesized using a modified version of the procedure first reported by Brust et al.[20, 21] Two separate reaction batches were prepared; the first one was stopped at an early time to obtain nanoparticles with an average diameter of 1.8 nm, as measured from image analysis STEM micrographs. The surface of these nanoparticles was passivated with thiol-terminated polystyrene chains with molecular weight of 1000g/mol. The second batch was allowed to react until the average nanoparticle core size reached an average value of 5 nm. This batch was divided in two fractions, for addition of different ligands, namely 1000 g/mol PS and 50000 g/mol PS.

The resulting toluene nanoparticle solutions were cleaned by precipitating them from the solution using methanol. This procedure was repeated at least 8 times. After cleaning, thermogravimetric analysis was performed to obtain the grafting densities of the nanoparticles.

The average size of the particles was obtained using a JEOL 2010 transmission electron microscope (TEM) operating at an accelerating voltage of 200KV in scanning mode using a high-angle annular dark-field detector (HAADF). TEM grids were prepared by evaporating dilute solutions of the nanoparticles. After imaging, the diameter of the particles was estimated from measurement of over 300 particles, using Image J software.

4.2.2 Sample Preparation

After characterization, the nanoparticle solutions were mixed with previously prepared toluene solutions of polystyrene homopolymer of M_n = 130,000 g/mol, 152,000 g/mol, and 900,000 g/mol. The nanocomposite solutions had compositions ranging from 0.1 to 5% by weight of gold cores for the case of the nanoparticles with 1000 g/mol PS ligands, and from 0.1 to 10% for the nanoparticles with 50,000 g/mol ligands. Each of the nanocomposites can be characterized by the relative size of the ligand (N, which denotes number of monomer units) and matrix chains (denoted as P), as well as by the ratio of R_e/R_g (see Table 1). Here, R_g refers to the unperturbed radius of gyration of the host chains, and R_e refers to the effective particle radius, which is given by the gold core radius and the brush thickness. The values of R_e were obtained by measuring interparticle separation distance on TEM samples of the pure particles.

The nanocomposite solutions described above were spin-coated on Si_3N_4 substrates to obtain film thicknesses between 100 and 115 nm. The thickness of the films was measured by ellipsometry using a J. A. Woollam M-44 variable-angle spectroscopic ellipsometer with a visible light source (wavelengths from 400 to 720nm). After spin coating, the resulting films were placed in an oven at 80°C for 48 hours under a vacuum to remove residual solvent. At this point, it is important to note that the samples were not annealed at a higher temperature to avoid nanoparticle coarsening which has been observed for similar systems.[22]

The depth profile of gold within the samples was characterized using dynamic secondary ion-mass spectroscopy (DSIMS), measured at UCSB with a Physical Electronics 6650 Quadropole instrument. For DSIMS analysis, a second deuterated PS film was floated on top of the nanocomposite films to serve as a marker for the location of the free surface. Sputtering was then accomplished with a cesium primary ion beam

monitoring negative ions of Au, Si, D, and C. The sputtering time was converted to a depth scale using the depth profile and the total film thickness, measured from ellipsometry. The gold concentration is normalized by the total number of gold counts.

Finally, the degree of dispersion in the x-y plane of the films was characterized by obtaining STEM images of similar films cast on transparent silicon nitride membrane windows (SPI supplies).

4.2.3 Glass Transition Temperature Measurements

After sample annealing, the samples were placed in a custom made heating stage, and their thickness was measured at regular intervals of 10°C during the experiment. Three measurements were taken at each temperature. The heating rate was 1°C/min, and the temperature ramp started at 30°C and ended at 170°C. Film thickness was determined by fitting the ellipsometric angles, Δ and Ψ, to a composite layer (effective medium approximation) of a Cauchy model and gold, using the Maxwell-Garnett model. T_g was determined by fitting straight lines through the data in the glassy and rubbery regions, respectively, the temperature at which these lines intersect denotes the glass transition.

Table 4.1. Characteristics of the Film Nanocomposites

Sample	Nanoparticle	h (nm)	P	N	R_{Au}/R_g	R_e/R_g	$\sigma N^{1/2}$	$(N/P)^2$
A	Au(5)-PS_{10}-SH	117	1462	9.6	0.24	0.48	1.13	$4.32*10^{-5}$
B	Au(5)-PS_{481}-SH	96	1462	481	0.23	2.6	9.55	0.11
C	Au(2)-PS_{10}-SH	107	1462	9.6	0.088	0.22	1.67	$4.32*10^{-5}$

4.3 RESULTS.

In figure 4.1, we present the concentration dependent glass transition of the films prepared for the study. The T_g is normalized with respect to that reported for relatively thick (100nm) PS films. For ease of discussion, we will label the three series of samples as follows: A samples correspond to nanocomposites with D_{core} =5 nm, N = 10 and P = 1300; B samples correspond to nanocomposites with D_{core}= 5nm, N = 480, and P = 1300; finally, C samples correspond to nanocomposites with D_{core} = 1.8 nm, N = 10 and P = 1500. From the plot, it is readily observed that it is possible to control the glass transition of the films simply controlling the relative magnitudes of the molecular dimensions involved in the system. For example, we observe that the A samples show a marked increase of the glass transitions at low nanoparticle loadings, reaching a maximum at mass fraction of 0.02 and subsequently decreasing sharply to the typical value for a pure PS film. B samples show no change in T_g even at comparatively high loadings of nanoparticles. Finally, C samples show a big contrast with respect to the other samples, as their glass transition is observed to decrease sharply upon nanoparticle addition.

A first step towards understanding our results, is relating the compositional dependence of T_g to the internal structure of our films. We start off by describing the Au depth profile in the samples, which is a consequence of the entropic interactions between matrix and the polymer coated nanoparticles, as explained by Meli et al.[23]

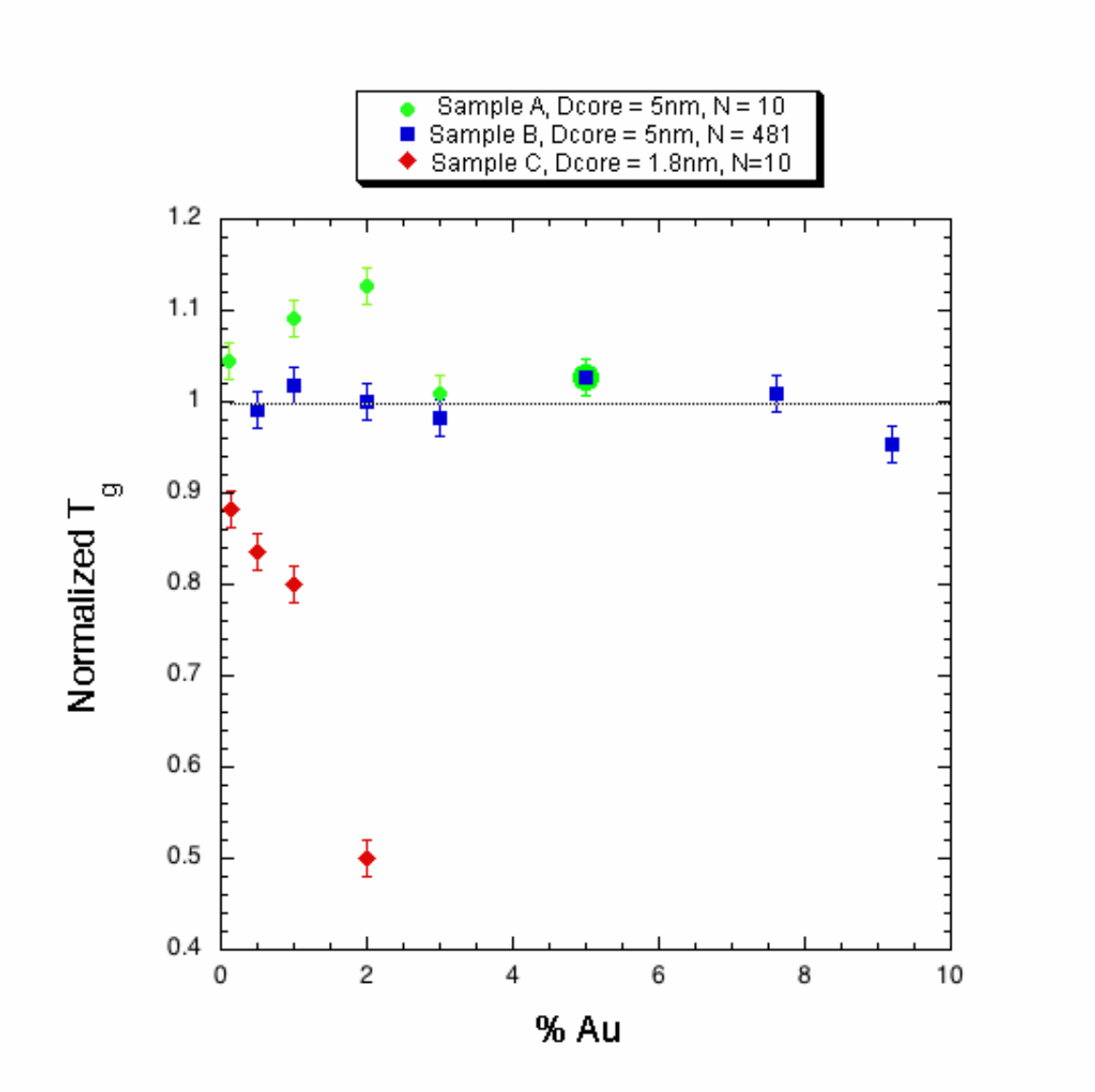

Figure 4.1 Dependence of T_g as a function of nanoparticle content. All films have thicknesses between 100 and 115 nm.

There are three main driving forces that determine the nanoparticle distribution across the film: 1) Entropy of mixing of the nanoparticles, which tends to promote dispersion across the film, and is inversely proportional to size of the nanoparticle, 2) restrictions on the conformational entropy of the matrix chains, which often lead to expulsion of the particles to the interfaces to avoid the stretching penalty incurred by having to stretch around the particles, and 3) entropic constraints due to brush-matrix chains interactions, which again can favor segregation of the particles to the interfaces if penetration of the matrix chains into the brush proves energetically unfavorable. The latter contribution is influenced by the degree of polymerization of the brush chains (N), the degree of polymerization of the melt (P), and the brush grafting density (σ). The combination of these three parameters determines the degree of penetration of the melt chains into the brush, and ultimately, the wetting behavior as explained by Ferreira and Leibler.[24] They show that when $\sigma(N)^{1/2} = (N/P)^2$, a wetting transition occurs delimiting the regions of negative and positive interfacial energy between the grafted and free chains. A positive interfacial tension leads to an effective repulsion between grafted and free chains, which can in turn lead to their phase separation. This wetting transition is different from the wet-to-dry brush transition; i.e. from the transition where mobile chains start to be expelled from the brush (the transition is located at $\sigma(N)^{1/2} = (P/N)^{-1/2}$ for $P/N < 1$ and at $\sigma(N)^{1/2} = 1$ for $P/N > 1$). We will use these relations as a guide to understand the entropic interactions in our system; however, it is important to note that they were derived for flat surfaces. In principle, a curved brush should be more penetrable by melt chains because the grafted chains are less stretched (and therefore less tightly packed) away from the particle surface. It is important to note that the above criteria tell us that all of our samples are in the dry brush regime.

Within this context, let us now discuss the depth profile of the particles in the films (Fig 4.2). Starting with the A samples, we see that the nanoparticles are exclusively segregated to the interfaces, which is an indication that due to their relatively large size (R_e/R_g = 0.48) and the large difference between the molecular weights of the matrix and grafted chains (P/N = 152 , which leads to non-wetting of the brush by the matrix $\sigma(N)^{1/2} >> (N/P)^2$) , the entropy of mixing of the nanoparticles is overcome by the loss of conformational entropy of the matrix chains. By allocating the nanoparticles at the interfaces this loss of conformational entropy is minimized, as depicted in figure 4.3b.

When the size of the nanoparticle is reduced (C samples, R_e/R_g =0.22), we find that their entropy of mixing increases in such a way that nanoparticles can be dispersed more readily throughout the whole film (Fig. 4.3a). Moreover, the lesser degree of stretching of the matrix chains that is expected for smaller fillers should also promote better dispersion. However, there is still some enrichment of the nanoparticles towards the interfaces. We believe this interfacial enrichment occurs because the polymer melt does not wet the short grafted chains covering the nanoparticle core, as in the previous case ($\sigma(N)^{1/2} >> (N/P)^2$).

Finally, we observe that a very uniform degree of dispersion was obtained in the B samples. We can attribute this result to the larger size of the grafted chains (P/N=3), which should allow for a greater interpenetration of the matrix and grafted chains. The greater degree of penetration should reduce the conformational entropy penalty of the matrix chains that would otherwise inhibit dispersion (Fig 4.3c). It is important to mention that according to the scaling theory for flat brushes, these grafted particles should not be wetted by the melt, since $\sigma(N)^{1/2} > (N/P)^2$.

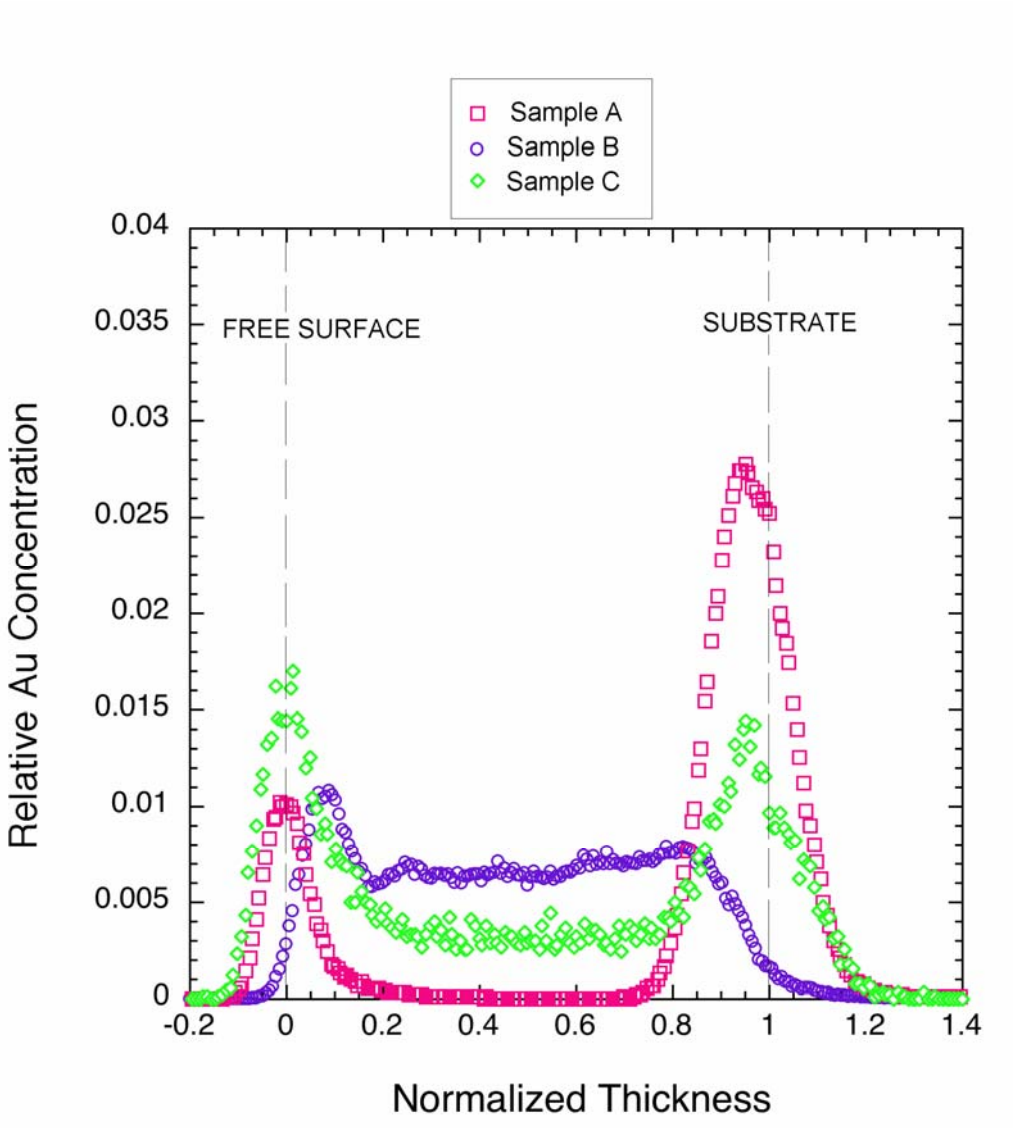

Figure 4.2 Depth distribution of gold content in the nanocomposite films determined by DSIMS. All samples were prepared with a gold content of 5% w/w.

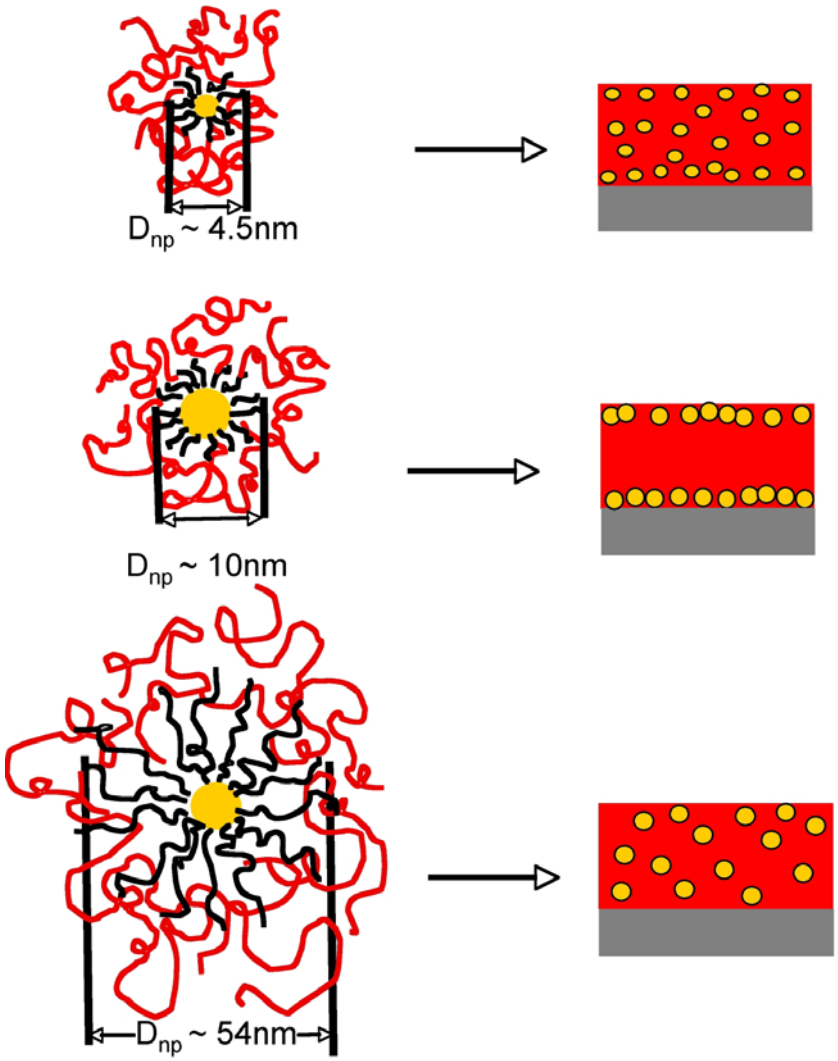

Figure 4.3 Schematic representation of the influence of core and ligand size on the depth distribution of the nanoparticles.

However, considering that the aforementioned condition is several orders of magnitude smaller for sample B ($\sigma(N)^{1/2}/ (N/P)^2 = O(10^1)$) than for samples A and C ($\sigma(N)^{1/2}/ (N/P)^2 = O(10^4)$), the resulting repulsive interaction between brush and free chains should be much weaker for sample B. Indeed, the high curvature of the brush in these particles might lead to complete wetting of the brush, as mentioned earlier.

The rationale for the observed glass transition is as follows. If we turn our attention to samples C, the brush surrounding this type of nanoparticles is highly incommensurate with the matrix chains. This results in a repulsive interaction between the matrix and the particle, which should in turn lead to a lower monomer density near the nanoparticle surface, as discussed in the introduction. However, as mentioned before, the high entropy of mixing of the nanoparticles allows them to be present throughout the sample, and therefore, a substantial amount of free volume is added to the film. This results in a lowering of the overall glass transition, i.e. this situation is analogous to mixing the matrix chains with small molecules or plasticizers.

In the B samples, we find a good degree of dispersion relative to the C samples. One could then naively conclude that the concentration dependence of T_g should be similar to what was observed in samples C; that is, one could perhaps expect the T_g to decrease with increasing particle concentration due to an increase in the free volume of the polymer film. Nonetheless, in this case, there is a greater degree of interpenetration of matrix and brush chains, and consequently a much less unfavorable interaction between them (perhaps even neutral interactions between brush and matrix). Hence, one can say that this is analogous to mixing homopolymer chains of comparable molecular weight, which should not change the dynamics of the film in an appreciable manner.

Finally, we discuss the results for the A samples. Here, the nanoparticles are exclusively segregated to the interfaces. The initial increase of the glass transition in

these samples can be understood as being a consequence of a loss of conformational entropy of the matrix chains located near the interfaces. That is, the addition of nanoparticles to the film effectively `pushes´ the matrix chains away from the free surface, where they have the highest degree of conformational freedom. This loss in conformational freedom results in an increase in the T_g of the film. One would expect that the effect should reach a plateau once the free surface is saturated. However, we see that this effect peaks at a nanoparticle concentration of 2% and subsequently decays. We can understand this by considering that after the nanoparticle concentration in the interfaces reaches its maximum value, addition of more nanoparticles results in their allocation in the interior of the film. In this case, we should recover to some extent the case in which free volume is added to the film due to the repulsive interactions between long matrix chains and the short ligands. Experiments to support this statement are shown in Figure 4.4, where the DSIMS profile for two A samples with different nanoparticle content, and the same original thickness are presented. We observe that the fraction of the film that has no nanoparticles has decreased from ~ 40% to ~ 20%.

Another factor that influences this behavior is the degree of dispersion within the film plane. Figure 4.5 shows STEM images for the three types of nanocomposite films prepared in this study; as can be seen, only the A samples present nanoparticle aggregation. This loss in property enhancement due to nanofiller aggregation has been observed before, although its contribution is expected to lead to a plateau in the measured property, rather than a decrease in it.[25]

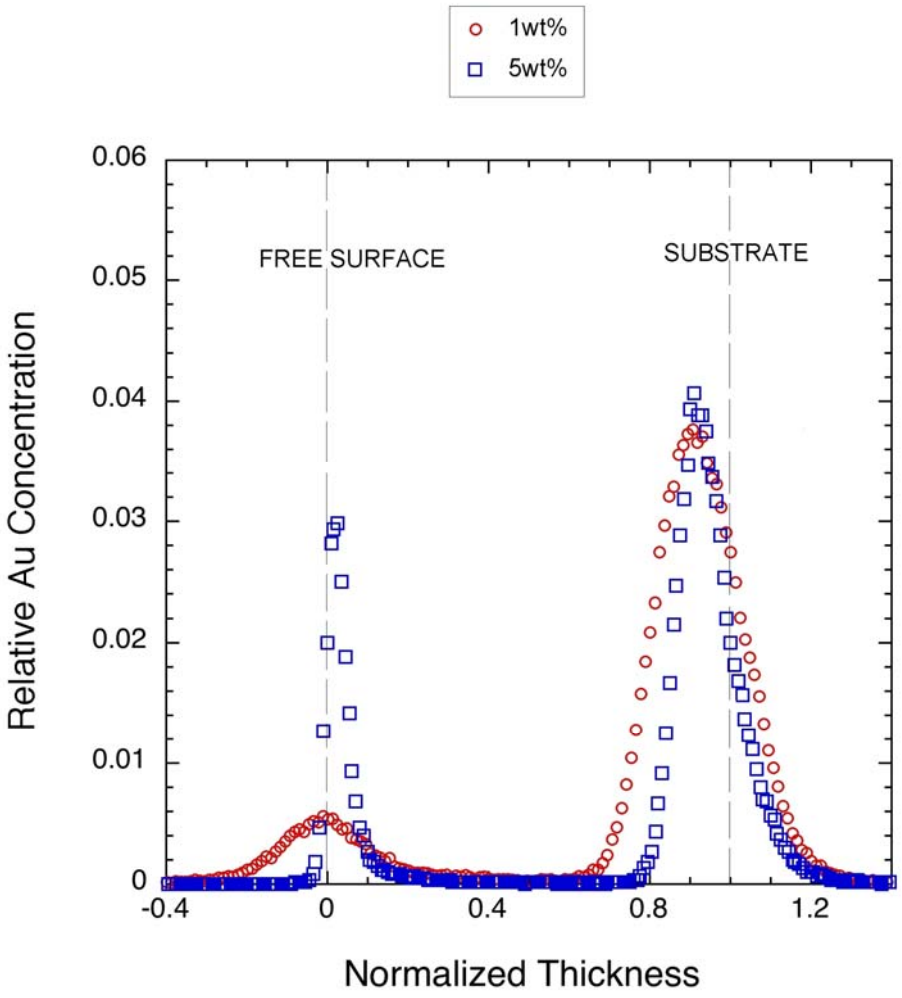

Figure 4.4 Effect of concentration on the depth profile of gold nanoparticles across film nanocomposites. Note the broadening of the gold signal at both interfaces, leading to a reduction of the 'nanoparticle' free film region.

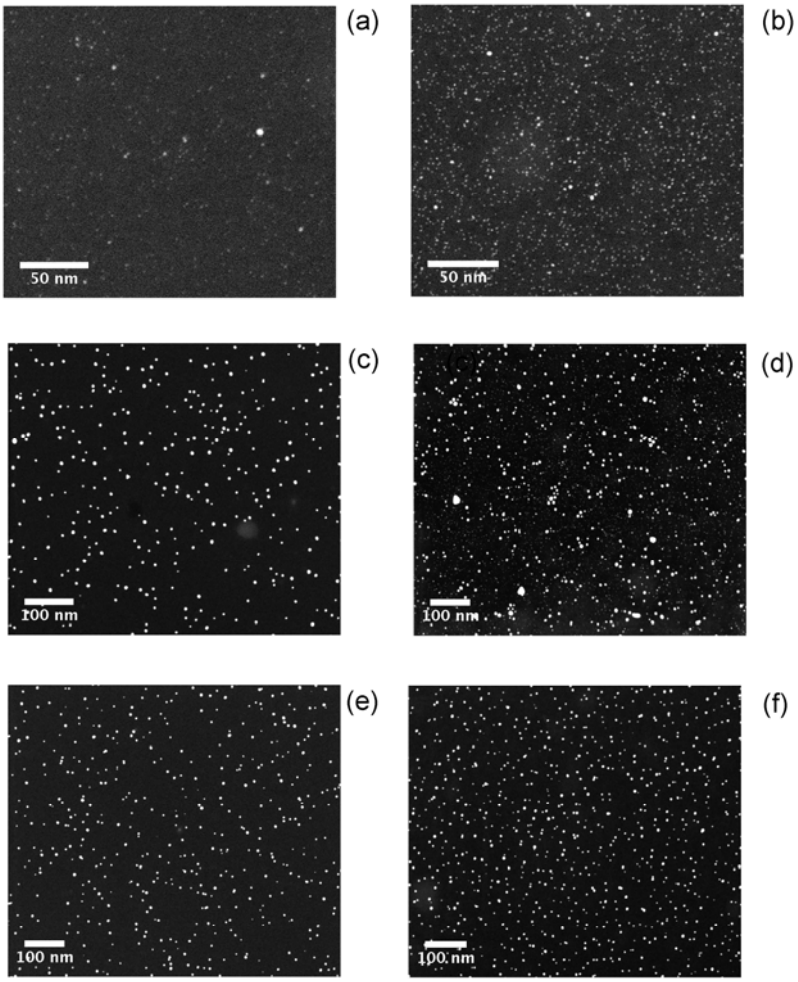

Figure 4.5 STEM images taken for152kPS/Au nanocomposites. The first row (a and b) corresponds to nanocomposites with gold nanoparticles characterized by D_{core} = 1.8 nm and N = 10. The second row (c and d) corresponds to nanocomposites with gold nanoparticles characterized by D_{core} = 5 nm and N = 10. The third row shows the nanocomposites formed with nanoparticles characterized by d = 5 nm and N = 480. The first column shows gold concentrations of 1% by weight, whereas the second shows images for gold concentration of 5%.

Finally, we can gain further insight into the behavior of the A samples by observing the change in T_g with decreasing thickness. As has been reported previously, the glass transition of PS films on non-wetting substrates is reduced with decreasing film thickness.[19] This does not happen in our nanocomposite films; instead, we are able to measure an increase in T_g of 10 K at a film thickness of 60 nm, even at a low nanoparticle weight fraction (Fig. 4.6). This result is consistent with the mechanism described above. Namely, the glass transition behavior is dominated by the interfaces of the film; as the film becomes thinner, the fraction of matrix polymer affected by the loss of conformational entropy is higher, resulting in an increase of T_g.

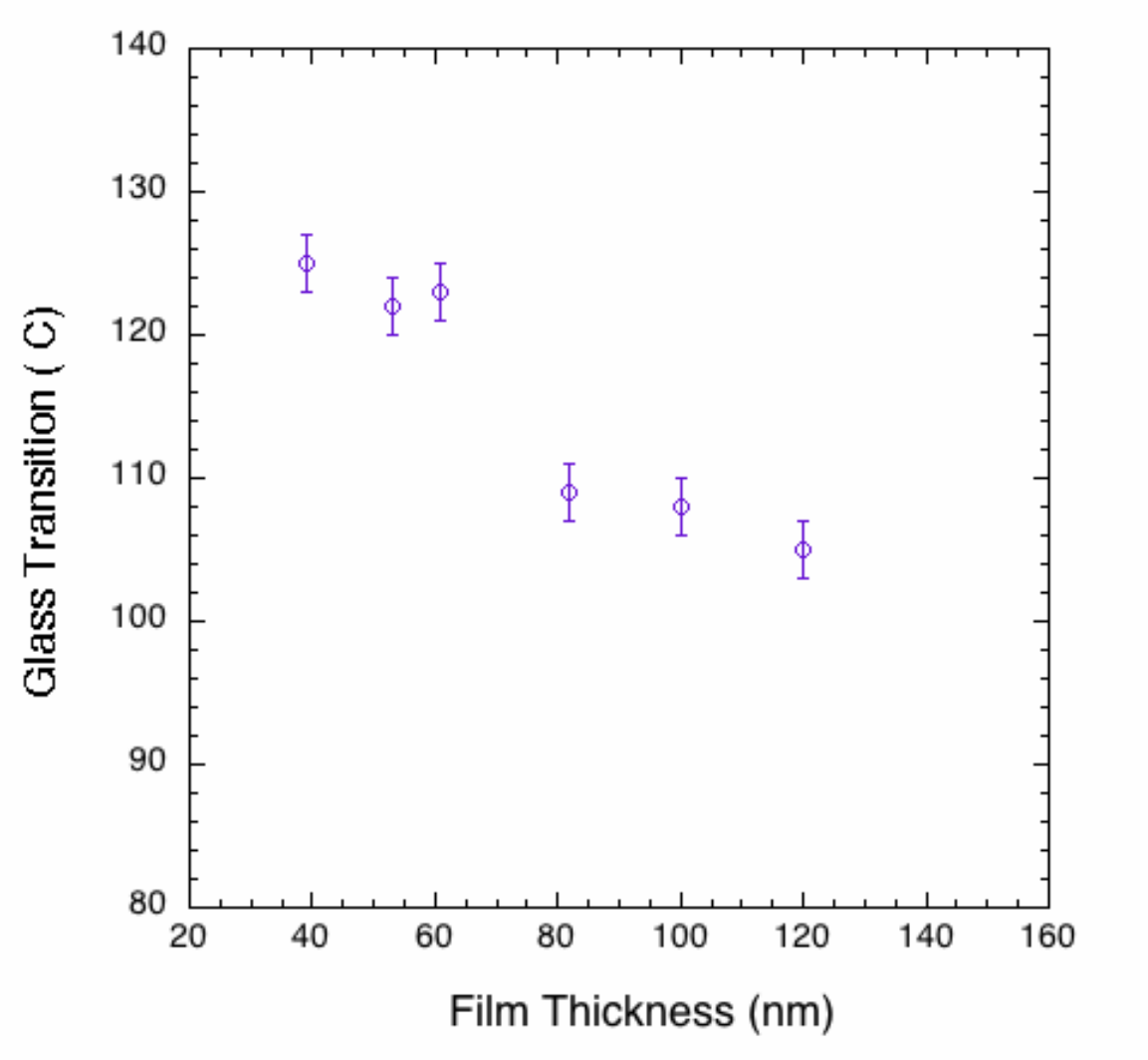

Figure 4.6. Glass transition of PS nanocomposites with 0.1% w/w $AuPS_{10}$, with 5 nm diameter, as a function of film thickness.

4.4 CONCLUSIONS

In this work, we studied the glass transition of polystyrene (PS) nanocomposite films filled with PS-coated nanoparticles. The focus of this study was to understand how different entropic interactions in the system affect the overall glass transition in the film. The entropic constraints present in the system are: i) penetrability of the brush by the matrix chains, ii) translational entropy of nanoparticles, and iii) loss of conformational entropy due to stretching of matrix chains around nanoparticles. Based on a previous description by Meli et al.,[23] we were able to correlate the measured T_g to the internal structure of the nanocomposite films. We found that nanoparticles coated with long chains, form a penetrable brush whose interactions with the matrix are small, thereby causing no appreciable changes in T_g. When the nanoparticles are coated with a short (impenetrable) brush, the effect of T_g will depend on the relative size of the nanoparticle (R_e) and matrix chain (R_g). For the case of small R_e / R_g, we observed that nanoparticles reduce the T_g of the film. The large translational entropy allows them to distribute across the film, and add free volume due to their non-wettable character. On the other hand, when R_e / R_g is large, the nanoparticles are primarily segregated to the interfaces, causing an increase in T_g at low concentrations. This effect decays at higher concentrations, due to a combined effect of nanoparticle aggregation, and addition of free volume due to penetration of the particles into the 'bulk' of the film.

4.5 REFERENCES

1. Ciprari, D.; Jacob, K.; Tannenbaum, R. *Macromolecules* **2006,** 39, (19), 6565-6573.

2. Berriot, J.; Montes, H.; Lequeux, F.; Long, D.; Sotta, P. *Macromolecules* **2002,** 35, (26), 9756-9762.

3. Bansal, A.; Yang, H. C.; Li, C. Z.; Cho, K. W.; Benicewicz, B. C.; Kumar, S. K.; Schadler, L. S. *Nature Materials* **2005,** 4, (9), 693-698.

4. Bansal, A.; Yang, H. C.; Li, C. Z.; Benicewicz, R. C.; Kumar, S. K.; Schadler, L. S. *Journal of Polymer Science Part B-Polymer Physics* **2006,** 44, (20), 2944-2950.

5. Ash, B. J.; Siegel, R. W.; Schadler, L. S. *Journal of Polymer Science Part B-Polymer Physics* **2004,** 42, (23), 4371-4383.

6. Savin, D. A.; Pyun, J.; Patterson, G. D.; Kowalewski, T.; Matyjaszewski, K. *Journal of Polymer Science Part B-Polymer Physics* **2002,** 40, (23), 2667-2676.

7. Pham, J. Q.; Mitchell, C. A.; Bahr, J. L.; Tour, J. M.; Krishanamoorti, R.; Green, P. F. *Journal of Polymer Science Part B-Polymer Physics* **2003,** 41, (24), 3339-3345.

8. Desai, T.; Keblinski, P.; Kumar, S. K. *Journal of Chemical Physics* **2005,** 122, (13), -.

9. Smith, G. D.; Bedrov, D.; Li, L. W.; Byutner, O. *Journal of Chemical Physics* **2002,** 117, (20), 9478-9489.

10. Starr, F. W.; Douglas, J. F.; Glotzer, S. C. *Journal of Chemical Physics* **2003,** 119, (3), 1777-1788.

11. Starr, F. W.; Schroder, T. B.; Glotzer, S. C. *Physical Review E* **2001,** 6402, (2), -.

12. Vacatello, M. *Macromolecules* **2001,** 34, (6), 1946-1952.

13. Pryamitsyn, V.; Ganesan, V. *Macromolecules* **2006,** 39, (2), 844-856.

14. McCoy, J. D.; Curro, J. G. *Journal of Chemical Physics* **2002,** 116, (21), 9154-9157.

15. Long, D.; Lequeux, F. *European Physical Journal E* **2001,** 4, (3), 371-387.

16. Kim, J. H.; Jang, J.; Zin, W. C. *Langmuir* **2000,** 16, (9), 4064-4067.

17. Kim, J. H.; Jang, J.; Lee, D. Y.; Zin, W. C. *Macromolecules* **2002,** 35, (1), 311-313.

18. Keddie, J. L.; Jones, R. A. L.; Cory, R. A. *Europhysics Letters* **1994,** 27, (1), 59-64.

19. Keddie, J. L.; Jones, R. A. L.; Cory, R. A. *Faraday Discussions* **1994**, (98), 219-230.

20. Brust, M.; Walker, M.; Bethell, D.; Schiffrin, D. J.; Whyman, R. *Journal of the Chemical Society. Chemical Communications* **1994**, 801.

21. Brust, M.; Fink, J.; Bethell, D.; Schiffrin, D. J.; Kiely, C. *Journal of the American Chemical Society* **1995,** Communications, 1655.

22. Meli, L.; Johnston, K. P.; Green, P. F. *Journal of Chemical Physics* **2007,** Submitted.

23. Meli, L.; Green, P. F. Microstrutcture design and formation of thin film polymer nanocomposites. University of Texas at Austin, Austin, 2007.

24. Ferreira, P. G.; Ajdari, A.; Leibler, L. *Macromolecules* **1998,** 31, (12), 3994-4003.

25. Kropka, J. M.; Putz, K. W.; Pryamitsyn, V.; Ganesan, V.; Green, P. F. *Macromolecules* **2007,** To be published.

Chapter 5. Conclusions and Recommendations for Future Work

5.1 CONCLUSIONS

The versatility of polymers comes from the wide range of properties endowed by their structural and chemical diversity. The morphological characteristics of bulk polymer systems are connected to this diversity, as well as to processing. With regard to thin films, their physical properties, as well as their morphology, are strongly influenced by confinement and interfacial interactions. The latter is of particular significance as thin polymers in the nanometer thickness range have a wide range of applications, from patterning to device applications. The work presented in this dissertation examined the behavior of thermally induced transitions in two polymer-based thin film systems, an A-b-B diblock copolymer and an amorphous polymer filled with particles of nanoscale dimensions. Three problems were examined specifically: (1) the role of supercritical CO_2 on the isotropic-to-lamellar transition in a symmetric poly(styrene-b-methyl methacrylate) PS-b-PMMA diblock copolymer thin film; (2) the influence of PS-grafted gold nanoparticles on the ODT of PS-b-PMMA diblock copolymers and (3) the influence of the composition and of the spatial distribution of PS-grafted gold nanoparticles on the T_g of PS films of varying compositions.

5.1.1 Order-Disorder Transition Temperature of Thin Diblock Copolymer Films

In Chapter 2 of this dissertation we explored, separately, the effects of confinement and sorption of supercritical carbon dioxide, $scCO_2$, on the order-disorder

transition temperature of thin films of symmetric poly(styrene-b-methyl methacrylate) (PS-*b*-PMMA) diblock copolymers. First, we show that the ordering temperature of thin films of PS-*b*-PMMA with thickness $h \leq 2L$, supported by SiO_x/Si substrates, in vacuum environments, increases beyond the bulk value. Estimates of the temperature shifts indicate that small increases of χN are associated with unusually large shifts of the ODT to higher T. More specifically, the presence of interfaces in this system forces a reduction in the transition to $7.6 < \chi N_{ODT} < 7.9$, compared to the bulk value of $\chi N_{ODT} = 10.5$. This shift in the χN_{ODT} value implies an increase of more than 100 °C in the ordering temperature for PS-b-PMMA. The strong interaction between the PMMA block and the silicon substrate (and to a lesser extent, to the preferential affinity of the PS block for the free surface) enhances phase separation by increasing the 'effective' incompatibility between the two constituent blocks.

The next step was to subject thin films of PS-b-PMMA to $scCO_2$ annealing. We find that in compressed CO_2 environments, these films are ordered at temperatures where the films are disordered in vacuum (or air) environments. The results found are unexpected, since small molecule diluents – specifically $scCO_2$ – are known to decrease T_{ODT} by screening unfavorable enthalpic interactions in bulk diblock copolymer systems with an upper order-disorder transition temperature (UODT), as is the case of PS-b-PMMA. We rationalize our observations by considering that $scCO_2$ is highly selective towards the PMMA block. Furthermore, there is evidence that suggests that the selectivity of $scCO_2$ for PMMA is exacerbated in thin films. Thus, upon absorption of the supercritical fluid, the PMMA is swollen considerably more than the PS block, leading to a free volume mismatch between them, which is a known driving force for microphase segregation in diblock copolymers. Our results were later corroborated by

means of molecular simulations, probing the effect of a selective solvent on the ODT of swollen diblock copolymer films[1].

Block copolymer nanocomposites are particularly important due to their potential to enable cutting-edge applications in fields like photonics, photovoltaics, and sensing technologies. Inspired by the many application of these materials, we revisited the order-disorder transition temperature of PS-b-PMMA thin films in Chapter 3, this time considering block copolymer nanocomposite films supported by silicon nitride (Si_3N_4) substrates. The goal of this research was to study the effect of adding selective nanoparticles of size comparable to the lamellar spacing (L) on the phase behavior of the diblock. Our most significant finding is that the order-disorder transition of the nanocomposite films is reduced beyond what is expected for the neat block copolymer films ($\chi N < 7.6$) at the same experimental conditions. To the best of our knowledge, this is the first time that enhancement of phase segregation of thin block copolymer films by nanoparticles is reported. Recent theoretical results by Fredrickson and coworkers[2], however, give us some insight into the possible mechanism that enhances phase segregation in our system. Briefly, the authors show that a single selective nanoparticle immersed within a diblock copolymer can induce an enrichment of the favorably interacting block around its surface. Additionally, they demonstrate that interactions between two particles embedded in the diblock can propagate this effect at distances of several R_g. Further insight can be gained by comparing our results to theoretical predictions[3, 4] of the phase behavior of A-b-B symmetric diblock copolymer/A homopolymer blends where addition of homopolymer chains with degrees of polymerization greater than that of the selective block reduces the ordering transition due to restriction of the A block conformational entropy.

5.1.2 Glass Transition of Thin Film Nanocomposites

In Chapter 4, we studied the glass transition of PS films filled with PS-coated gold nanoparticles supported on Si_3N_4 substrates. The model thin film system that was chosen allowed the in-plane and depth distributions of the nanoparticles to be well-controlled and easily characterized, facilitating the formulation of structure-property relations.

First, the internal structure of the films is explained to be a consequence of three main entropic interactions: (i) the translational entropy of the nanoparticles, (ii) the entropic interactions between the brush covering the nanoparticles and the matrix chains, and (iii) the loss of conformational entropy of the matrix chains due to chain stretching around the nanoparticles. Knowledge of the interplay between these three entropic interactions allows us obtain different nanoparticle distributions by simple manipulation of the brush characteristics and the size of the nanoparticle core.

When the nanoparticles are allowed into the inteior of the film, the interactions between the brush and the matrix chains dominate glass transition behavior. For the case of long grafted chains, T_g does not change appreciably because the matrix chains can penetrate into the brush, which implies that their conformational entropy is not significantly restricted. Thus, this case is analogous to mixing two polymers of comparable molecular weight, which are known to cause no appreciable change in the T_g of the polymer. On the other hand, nanoparticles grafted with very short polymer chains form an impenetrable 'dry' brush, which is not wetted by the matrix chains. The effective repulsion between brush and matrix caused by the non-wetting condition leads to an increase in the free volume of the polymer upon introduction of the particles into the film. Finally, when the interactions in the film force the nanoparticles primarily to

the interfaces, we find that T_g increases at low concentrations until a maximum is reached, and then recovers the value of a neat PS film. The increase in T_g can be explained by loss of conformational entropy of the matrix chains as they are displaced from the region of the film with highest configurational freedom: the free surface. On the other hand we propose that the recovery of T_g has to do with a combined effect of aggregation between nanoparticles at the surface, accompanied by the penetration of filler to the interior of the film at higher particle concentrations, resulting in an increase in the free volume of the system.

5.2 RECOMMENDATIONS FOR FUTURE WORK

5.2.1 Order disorder transition temperature of diblock copolymer films

In the following, we give a brief description of some of the projects presented in this dissertation which could benefit from further research.

ODT of block copolymer films under compressed environments. Due to limitations in the available molecular weights of our diblock copolymers, our results do not show how low the molecular weight of the films has to be to encounter a phase mixing. It would be interesting to find the limit of this segregation enhancement, since diblock copolymer films are often used as photolithographic masks. Thus, being able to produce smaller features from phase segregated diblock films is relevant from a technological standpoint. Another important question arising from this study is whether a compressible gas with a different degree of selectivity can shift the ODT in the same magnitude, or in the same direction as $scCO_2$. It would therefore be interesting to explore this issue by conducting experiments with a supercritical gas such as xenon, which should have no specific interaction with either one of the blocks, and which has an accessible supercritical point. One could then perform analogous experiments with supercritical

ethane, which should be selective towards the PS block. The results emerging from these experiments would provide valuable insight into the processability of diblock thin films for industrial applications.

ODT of block copolymer nanocomposite films. The results obtained from our work in this area could be enriched by exploring the influence of the vast parameter space that a complex system like this provides. A starting point could be modifying characteristics of the brush layer covering the nanoparticles, by using different molecular weights, and grafting densities. Another option here would be to find a non-selective nanoparticle that could migrate to the A/B interface and become a driving force for phase mixing in the system. Alternatively, this research could also include the effects of nanoparticles on the ordering transition films prepared with asymmetric block copolymers. Here, it is possible to find out whether this effect is the same if nanoparticles are added to the minority component in the chain versus adding them to the majority component. This could potentially give rise to the alteration of the microdomain morphology.

5.2.2 Glass Transition of Nanocomposite Films

The results obtained in this part of the dissertation underscore the need to continue research in the glass transition of polymer films filled with 'hairy' nanoparticles. Perhaps the most obvious step would be to find out whether our results are a consequence of a general behavior. Therefore, we propose to carry out experiments to verify if this behavior can be scaled to other nanoparticle sizes, and other ligand and matrix molecular weights. This has the potential to provide us with general guidelines to tune the glass

transition temperature of a polymer. Currently, there is not enough available data in the literature to make assumptions about the generality of the effects described in Chapter 4.

As in the previous recommendation for diblock nanocomposite films, the ability to modify the characteristics of the brush offers a wide range of variables that can help control with a great degree of accuracy the glass transition of this type of systems. A very interesting, albeit complex situation to study would be the addition of enthalpic interactions into our nanocomposites. What happens when there is a strongly repulsive ligand decorating the surfaces of the nanoparticles? A short series of preliminary experiments performed by us (not included in this dissertation) shows that poly(2-vinyl pyridine) (P2VP)-coated nanoparticles shift the T_g to even larger values than nanoparticles coated with short PS chains. This result is counterintuitive, if one considers that hard (without a brush) repulsive surfaces have been shown to lower the glass transition of homopolymer films. Much more experimentation has to be performed in this regard before we can elucidate the mechanisms that engender this atypical behavior.

5.3 REFERENCES

1. Shah, M.; Pryamitsyn, V.; Ganesan, V. *Journal of Physical Chemistry B* **2007,** 111, (2), 402-407.

2. Reister, E.; Fredrickson, G. H. *Macromolecules* **2004,** 37, (12), 4718-4730.

3. Likhtman, A. E.; Semenov, A. N. *Macromolecules* **1997,** 30, (23), 7273-7278.

4. Matsen, M. W. *Macromolecules* **1995,** 28, (17), 5765-5773.

References

1. Anastasiadis, S. H.; Russell, T. P.; Satija, S. K.; Majkrzak, C. F. *Physical Review Letters* **1989,** 62, (16), 1852-1855.

2. Arceo, A.; Green, P. F. *Journal of Physical Chemistry B* **2005,** 109, (15), 6958-6962.

3. Ash, B. J.; Siegel, R. W.; Schadler, L. S. *Journal of Polymer Science Part B-Polymer Physics* **2004,** 42, (23), 4371-4383.

4. Bansal, A.; Yang, H. C.; Li, C. Z.; Benicewicz, R. C.; Kumar, S. K.; Schadler, L. S. *Journal of Polymer Science Part B-Polymer Physics* **2006,** 44, (20), 2944-2950.

5. Bansal, A.; Yang, H. C.; Li, C. Z.; Cho, K. W.; Benicewicz, B. C.; Kumar, S. K.; Schadler, L. S. *Nature Materials* **2005,** 4, (9), 693-698.

6. Bates, F. S.; Fredrickson, G. H. *Annual Review of Physical Chemistry* **1990,** 41, 525-557.

7. Berriot, J.; Montes, H.; Lequeux, F.; Long, D.; Sotta, P. *Macromolecules* **2002,** 35, (26), 9756-9762.

8. Black, C. T.; Guarini, K. W.; Milkove, K. R.; Baker, S. M.; Russell, T. P.; Tuominen, M. T. *Applied Physics Letters* **2001,** 79, (3), 409-411.

9. Bliznyuk, V.; Ruhstaller, B.; Brock, P. J.; Scherf, U.; Carter, S. A. *Advanced Materials* **1999,** 11, (15), 1257-+.

10. Bockstaller, M. R.; Mickiewicz, R. A.; Thomas, E. L. *Advanced Materials* **2005,** 17, (11), 1331-1349.

11. Brochard-Wyart, F.; de Gennes, P. G. *The European Physical Journal E* **2000,** 1, 93-97.

12. Brust, M.; Fink, J.; Bethell, D.; Schiffrin, D. J.; Kiely, C. *Journal of the American Chemical Society* **1995,** Communications, 1655.

13. Brust, M.; Walker, M.; Bethell, D.; Schiffrin, D. J.; Whyman, R. *Journal of the Chemical Society. Chemical Communications* **1994**, 801.

14. Buxton, G. A.; Lee, J. Y.; Balazs, A. C. *Macromolecules* **2003,** 36, (25), 9631-9637.

15. Chervanyov, A. I.; Balazs, A. C. *Journal of Chemical Physics* **2003,** 119, (6), 3529-3534.

16. Chiu, J. J.; Kim, B. J.; Kramer, E. J.; Pine, D. J. *Journal of the American Chemical Society* **2005,** 127, (14), 5036-5037.

17. Chou, S. Y.; Wei, M. S.; Krauss, P. R.; Fischer, P. B. *Journal of Applied Physics* **1994,** 76, (10), 6673-6675.

18. Ciprari, D.; Jacob, K.; Tannenbaum, R. *Macromolecules* **2006,** 39, (19), 6565-6573.

19. de Gennes, P. G. *The European Physical Journal E* **2000,** 2, 201-205.

20. De Rosa, C.; Park, C.; Thomas, E. L.; Lotz, B. *Nature* **2000,** 405, (6785), 433-437.

21. Desai, T.; Keblinski, P.; Kumar, S. K. *Journal of Chemical Physics* **2005,** 122, (13), -.

22. Ellison, C. J.; Ruszkowski, R. L.; Fredin, N. J.; Torkelson, J. M. *Physical Review Letters* **2004,** 92, (11), -.

23. Ellison, C. J.; Torkelson, J. M. *Nature Materials* **2003,** 2, (10), 695-700.

24. Erichsen, J.; Kanzow, J.; Schurmann, U.; Dolgner, K.; Gunther-Schade, K.; Strunskus, T.; Zaporojtchenko, V.; Faupel, F. *Macromolecules* **2004,** 37, (5), 1831-1838.

25. Ferreira, P. G.; Ajdari, A.; Leibler, L. *Macromolecules* **1998,** 31, (12), 3994-4003.

26. Forrest, J. A.; DalnokiVeress, K.; Dutcher, J. R. *Physical Review E* **1997,** 56, (5), 5705-5716.

27. Fredrickson, G. H. *Macromolecules* **1987,** 20, (10), 2535-2542.

28. Gebremichael, Y.; Vogel, M.; Bergroth, M. N. J.; Starr, F. W.; Glotzer, S. C. *Journal of Physical Chemistry B* **2005,** 109, (31), 15068-15079.

29. Green, P. F. *Journal of Polymer Science Part B-Polymer Physics* **2003,** 41, (19), 2219-2235.

30. Guarini, K. W.; Black, C. T.; Milkove, K. R.; Sandstrom, R. L. *Journal of Vacuum Science & Technology B* **2001,** 19, (6), 2784-2788.

31. Hamdoun, B. *European Polymer Journal* **2004,** 40, (7), 1559-1564.

32. Hamley, I. W., *The physics of block copolymers*. Oxford University Press: Oxford, 1998.

33. Helfand, E. *Macromolecules* **1975,** 8, (4), 552-556.

34. Helfand, E.; Wasserman, Z. R. *Macromolecules* **1976,** 9, (6), 879-888.

35. Huang, F.; Zhang, H. Z.; Banfield, J. F. *Journal of Physical Chemistry B* **2003,** 107, (38), 10470-10475.

36. Huh, J.; Ginzburg, V. V.; Balazs, A. C. *Macromolecules* **2000,** 33, (21), 8085-8096.

37. Jain, A.; Gutmann, J. S.; Garcia, C. B. W.; Zhang, Y. M.; Tate, M. W.; Gruner, S. M.; Wiesner, U. *Macromolecules* **2002,** 35, (13), 4862-4865.

38. Keddie, J. L.; Jones, R. A. L.; Cory, R. A. *Europhysics Letters* **1994,** 27, (1), 59-64.

39. Keddie, J. L.; Jones, R. A. L.; Cory, R. A. *Faraday Discussions* **1994**, (98), 219-230.

40. Kim, B. J.; Chiu, J. J.; Yi, G. R.; Pine, D. J.; Kramer, E. J. *Advanced Materials* **2005,** 17, (21), 2618-+.

41. Kim, J. H.; Jang, J.; Lee, D. Y.; Zin, W. C. *Macromolecules* **2002,** 35, (1), 311-313.

42. Kim, J. H.; Jang, J.; Zin, W. C. *Langmuir* **2000,** 16, (9), 4064-4067.

43. Kim, J. H.; Jang, J.; Zin, W. C. *Langmuir* **2001,** 17, (9), 2703-2710.

44. Kim, J. U.; O'Shaughnessy, B. *Macromolecules* **2006,** 39, (1), 413-425.

45. Klos, J.; Pakula, T. *Macromolecules* **2004,** 37, (21), 8145-8151.

46. Krishnamoorti, R.; Giannelis, E. P. *Macromolecules* **1997,** 30, (14), 4097-4102.

47. Krishnamoorti, R.; Yurekli, K. *Current Opinion in Colloid & Interface Science* **2001,** 6, (5-6), 464-470.

48. Krishnan, R. S.; Mackay, M. E.; Hawker, C. J.; Van Horn, B. *Langmuir* **2005,** 21, (13), 5770-5776.

49. Kropka, J. M.; Putz, K. W.; Pryamitsyn, V.; Ganesan, V.; Green, P. F. *Macromolecules* **2007,** To be published.

50. Lee, J. Y.; Shou, Z. Y.; Balazs, A. C. *Macromolecules* **2003,** 36, (20), 7730-7739.

51. Leibler, L. *Macromolecules* **1980,** 13, (6), 1602-1617.

52. Li, C. X.; Wu, J. T.; Zhao, J.; Zhao, D. L.; Fan, Q. R. *European Polymer Journal* **2004,** 40, (8), 1807-1814.

53. Likhtman, A. E.; Semenov, A. N. *Macromolecules* **1997,** 30, (23), 7273-7278.

54. Limary, R.; Green, P. F. *Langmuir* **1999,** 15, (17), 5617-5622.

55. Limary, R.; Green, P. F. *Macromolecules* **2002,** 35, (17), 6486-6489.

56. Limary, R.; Green, P. F.; Shull, K. R. *European Physical Journal E* **2002,** 8, (2), 103-110.

57. Long, D.; Lequeux, F. *European Physical Journal E* **2001,** 4, (3), 371-387.

58. Mackay, M. E.; Dao, T. T.; Tuteja, A.; Ho, D. L.; Van Horn, B.; Kim, H. C.; Hawker, C. J. *Nature Materials* **2003,** 2, (11), 762-766.

59. Mackay, M. E.; Tuteja, A.; Duxbury, P. M.; Hawker, C. J.; Van Horn, B.; Guan, Z. B.; Chen, G. H.; Krishnan, R. S. *Science* **2006,** 311, (5768), 1740-1743.

60. Mansky, P.; Tsui, O. K. C.; Russell, T. P.; Gallot, Y. *Macromolecules* **1999,** 32, (15), 4832-4837.

61. Matsen, M. W. *Macromolecules* **1995,** 28, (17), 5765-5773.

62. McCoy, J. D.; Curro, J. G. *Journal of Chemical Physics* **2002,** 116, (21), 9154-9157.

63. Meli, L.; Green, P. F. Microstrutcture design and formation of thin film polymer nanocomposites. University of Texas at Austin, Austin, 2007.

64. Meli, L.; Johnston, K. P.; Green, P. F. *Journal of Chemical Physics* **2007,** Submitted.

65. Menelle, A.; Russell, T. P.; Anastasiadis, S. H.; Satija, S. K.; Majkrzak, C. F. *Physical Review Letters* **1992,** 68, (1), 67-70.

66. Mittal, J.; Shah, P.; Truskett, T. M. *Journal of Physical Chemistry B* **2004,** 108, (51), 19769-19779.

67. Morita, H.; Tanaka, K.; Kajiyama, T.; Nishi, T.; Doi, M. *Macromolecules* **2006,** 39, (18), 6233-6237.

68. Orso, K. A.; Green, P. F. *Macromolecules* **1999,** 32, (4), 1087-1092.

69. Pai, R. A.; Humayun, R.; Schulberg, M. T.; Sengupta, A.; Sun, J. N.; Watkins, J. J. *Science* **2004,** 303, (5657), 507-510.

70. Papakonstantopoulos, G. J.; Yoshimoto, K.; Doxastakis, M.; Nealey, P. F.; de Pablo, J. J. *Physical Review E* **2005,** 72, (3), -.

71. Park, M.; Harrison, C.; Chaikin, P. M.; Register, R. A.; Adamson, D. H. *Science* **1997,** 276, (5317), 1401-1404.

72. Pham, J. Q.; Green, P. F. *Journal of Chemical Physics* **2002,** 116, (13), 5801-5806.

73. Pham, J. Q.; Green, P. F. *Macromolecules* **2003,** 36, (5), 1665-1669.

74. Pham, J. Q.; Johnston, K. P.; Green, P. F. *Journal of Physical Chemistry B* **2004,** 108, (11), 3457-3461.

75. Pham, J. Q.; Mitchell, C. A.; Bahr, J. L.; Tour, J. M.; Krishanamoorti, R.; Green, P. F. *Journal of Polymer Science Part B-Polymer Physics* **2003,** 41, (24), 3339-3345.

76. Pham, J. Q.; Sirard, S. M.; Johnston, K. P.; Green, P. F. *Physical Review Letters* **2003,** 91, (17), -.

77. Potschke, P.; Dudkin, S. M.; Alig, I. *Polymer* **2003,** 44, (17), 5023-5030.

78. Pryamitsyn, V.; Ganesan, V. *Macromolecules* **2006,** 39, (2), 844-856.

79. Pryamitsyn, V.; Ganesan, V. *Macromolecules* **2006,** 39, (24), 8499-8510.

80. RamachandraRao, V. S.; Gupta, R. R.; Russell, T. P.; Watkins, J. J. *Macromolecules* **2001,** 34, (23), 7923-7925.

81. RamachandraRao, V. S.; Watkins, J. J. *Macromolecules* **2000,** 33, (14), 5143-5152.

82. Reister, E.; Fredrickson, G. H. *Macromolecules* **2004,** 37, (12), 4718-4730.

83. Reister, E.; Fredrickson, G. H. *Journal of Chemical Physics* **2005,** 123, (21), -.

84. Riggleman, R. A.; Yoshimoto, K.; Douglas, J. F.; de Pablo, J. J. *Physical Review Letters* **2006,** 97, (4), -.

85. Savin, D. A.; Pyun, J.; Patterson, G. D.; Kowalewski, T.; Matyjaszewski, K. *Journal of Polymer Science Part B-Polymer Physics* **2002,** 40, (23), 2667-2676.

86. Schmaltz, B.; Brinkmann, M.; Mathis, C. *Macromolecules* **2004,** 37, 9056-9063.

87. Schultz, A. J.; Hall, C. K.; Genzer, J. *Macromolecules* **2005,** 38, (7), 3007-3016.

88. Shah, M.; Pryamitsyn, V.; Ganesan, V. *Journal of Physical Chemistry B* **2007,** 111, (2), 402-407.

89. Shull, K. R. *Macromolecules* **1992,** 25, (8), 2122-2133.

90. Shull, K. R. *Macromolecules* **1996,** 29, (7), 2659-2666.

91. Smith, A. P.; Douglas, J. F.; Meredith, J. C.; Amis, E. J.; Karim, A. *Physical Review Letters* **2001,** 8701, (1), -.

92. Smith, G. D.; Bedrov, D.; Li, L. W.; Byutner, O. *Journal of Chemical Physics* **2002,** 117, (20), 9478-9489.

93. Smith, M. D.; Green, P. F.; Saunders, R. *Macromolecules* **1999,** 32, (25), 8392-8398.

94. Stafford, C. M.; Russell, T. P.; McCarthy, T. J. *Macromolecules* **1999,** 32, (22), 7610-7616.

95. Starr, F. W.; Douglas, J. F.; Glotzer, S. C. *Journal of Chemical Physics* **2003,** 119, (3), 1777-1788.

96. Starr, F. W.; Schroder, T. B.; Glotzer, S. C. *Physical Review E* **2001,** 6402, (2), -.

97. Starr, F. W.; Schroder, T. B.; Glotzer, S. C. *Macromolecules* **2002,** 35, (11), 4481-4492.

98. Sternstein, S. S.; Zhu, A. J. *Macromolecules* **2002,** 35, (19), 7262-7273.

99. Thompson, R. B.; Ginzburg, V. V.; Matsen, M. W.; Balazs, A. C. *Science* **2001,** 292, (5526), 2469-2472.

100. Tran, T. A.; Said, S.; Grohens, Y. *Macromolecules* **2005,** 38, (9), 3867-3871.

101. Tsagaropoulos, G.; Eisenberg, A. *Macromolecules* **1995,** 28, (18), 6067-6077.

102. Tsagaropoulos, G.; Eisenberg, A. *Macromolecules* **1995,** 28, (1), 396-398.

103. Vacatello, M. *Macromolecules* **2001,** 34, (6), 1946-1952.

104. Vaia, R. A.; Giannelis, E. P. *Macromolecules* **1997,** 30, (25), 8000-8009.

105. Vogt, B. D.; Brown, G. D.; RamachandraRao, V. S.; Watkins, J. J. *Macromolecules* **1999,** 32, (23), 7907-7912.

106. Vogt, B. D.; RamachandraRao, V. S.; Gupta, R. R.; Lavery, K. A.; Francis, T. J.; Russell, T. P.; Watkins, J. J. *Macromolecules* **2003,** 36, (11), 4029-4036.

107. Wang, Q.; Nealey, P. F.; de Pablo, J. J. *Journal of Chemical Physics* **2003,** 118, (24), 11278-11285.

108. Watkins, J. J.; Brown, G. D.; RamachandraRao, V. S.; Pollard, M. A.; Russell, T. P. *Macromolecules* **1999,** 32, (23), 7737-7740.

109. Zhang, H. Z.; Banfield, J. F. *Nano Letters* **2004,** 4, (4), 713-718.

110. Zhang, Y.; Gangwani, K. K.; Lemert, R. M. *Journal of Supercritical Fluids* **1997,** 11, (1-2), 115-134.

Vita

Abraham Arceo was born in November 23, 1976 in Mexico City, Mexico, to Enrique Arceo Alcalá and Silvia de la Peña Rincón. After completing his High School studies at Escuela Mexicana Americana, in Mexico City, he enrolled at the National University of Mexico, majoring in Chemical Engineering. He graduated in June 2001 with a Bachelor of Science degree. During his graduation year, he worked at the Chemistry Institute in the National University of Mexico. Upon completion of his research work, he joined the research department of Grupo Comex.. In August 2001, he entered the Chemical Engineering program at The University of Texas, completing his M.S. degree in Chemical Engineering. He then entered the Materials Science and Engineering program at the University of Texas.

Permanent address: Pestalozzi 1110, Col. Del Valle
Mexico, D.F. 03100

This dissertation was typed by the author.